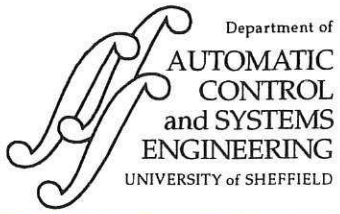

MODELLING AND PERFORMANCE ANALYSIS OF A FLEXIBLE MANIPULATOR SYSTEM USING SYMBOLIC MANIPULATION

Z Mohamed and M O Tokhi

Department of Automatic Control and Systems Engineering,
The University of Sheffield, Mappin Street, Sheffield, S1 3JD, UK.

Tel: + 44 (0)114 222 5617.
Fax: + 44 (0)114 222 5661.
E-mail: o.tokhi@sheffield.ac.uk.

Research Report No. 797

August 2001

Abstract

This paper presents a symbolic manipulation approach for modelling and performance analysis of a flexible manipulator system using finite element methods. A constrained planar single-link flexible manipulator is considered. A symbolic algorithm characterising the dynamic behaviour of the system is developed using a symbolic language. Using this approach, the system transfer functions are obtained in symbolic forms. Analyses and investigations in terms of system stability, time response to an input command and vibration frequencies are presented. Numeric and experimental results are presented for validation and assessment of the symbolic model.

Keywords: *Dynamic modelling, finite element method, flexible manipulator, symbolic manipulation.*

CONTENTS

LIST OF TABLES AND FIGURES

1. Introduction

Flexible robot manipulators exhibit several advantages over their rigid counterparts: they require less material, are lighter in weight, consume less power, require smaller actuators, are more manoeuvrable and transportable, have less overall cost and higher payload to robot weight ratio (Azad, 1995). However, control of flexible manipulators to maintain accurate positioning is an extremely challenging problem. Due to the flexible nature of the system, the dynamics are highly non-linear and complex. Problems arise due to difficulties in sensing the end-point displacement, vibration due to system flexibility, precise positioning requirement and the difficulty in obtaining accurate model for the system (Piedboeuf *et al.*, 1993; Yurkovich, 1992). Therefore, flexible manipulators have not been favoured in production industries, due to un-attained end-point positional accuracy in response to input commands. Thus, a control mechanism that accounts for both rigid body and flexural motions of the system is required.

The complexity of this problem increases dramatically when a flexible manipulator carries a payload. Practically, robots are required to perform a single or sequential task such as to pick up a payload, move to a specified location or along a pre-planned trajectory and place the payload. Previous investigations have shown that the dynamic behaviour of the manipulator is significantly affected by payload variations (Menq and Chen, 1988; Poerwanto, 1998). Thus, the effects of payload on the dynamic characteristics of the manipulator have to be studied and identified. If the advantages associated with lightness are not to be sacrificed, accurate models and efficient controllers have to be developed.

Various approaches have previously been developed for modelling of flexible manipulators (Azad, 1995). These include assumed modes (Book, 1984; Cannon and Schmitz, 1984; Hasting and Book, 1987), finite difference (FD) (Tokhi and Azad, 1995) and finite element (FE) methods (Aoustin *et al.*, 1994; Tokhi *et al.*, 1997; Usoro *et al.*, 1986) to solve the partial differential equation characterising the dynamic behaviour of a flexible manipulator system. Previous investigations have shown that the FE method can be utilised in obtaining a good representation of the system. It has also been reported that in using FE methods, a single element is sufficient to describe the dynamic behaviour of a flexible manipulator reasonably well. Using a single element, the first two modes of vibration are well described (Aoustin *et al.*, 1994). Moreover, the FE method exhibits several advantages over the FD method (Tokhi *et al.*, 1997).

Most of the investigations involving the FE method are numerical-based. Dynamic characteristics of the manipulator including stability, time response and vibration frequencies are interpreted on the basis of a single particular case, with no provision for any generality. Moreover, numerical systems must operate using numeric approximations, whose precision is limited by the computer hardware. Alternatively, exact quantities can be obtained by retaining the computations in a symbolic form. A distinguishing feature of symbolic-based methods is the mathematically comprehensive output they generate, so that the significance of individual terms, or group of terms, may be identified. This brings with it the opportunity to gain insights into the model that would otherwise not be available. A symbolic manipulation will open up the possibility of analysing a system in both new and interesting ways. It can be seen that the trend over time has been away from fully numeric methods of formulation towards those with a strong and total symbolic flavour to them. This is due to the overwhelmingly rapid improvements in computer hardware technology in general and in computer algebra software in particular (Larcombe and Brown, 1997).

Symbolic approaches for modelling and simulation of flexible manipulators have previously been investigated. Most of these investigations have developed automated symbolic derivations of dynamic equations of motion of rigid and flexible manipulators utilising Lagrangian formulation and assumed mode methods (Cetinkunt and Ittop, 1992; De Luca *et al.*, 1988; Lin and Lewis, 1994), Hamilton's principle and non-linear integro-differential equations (Low and Vidyasagar, 1988) and FD approximations (Tzes *et al.*, 1989). These have demonstrated that the approach has some advantages, such as allowing independent variation of flexure parameters. However, in utilising this manipulation approach, not much work has been done on modelling and analysis of a flexible manipulator using FE methods. Moreover, relations between system parameters including payload and hub inertia and the system characteristics have not been adequately addressed. The effect of payload on the manipulator is important for modelling and control purposes, as successful implementation of a flexible manipulator control is contingent upon achieving acceptable uniform performance in the presence of payload variations.

The aim of the work presented in this paper is to investigate the application of a symbolic manipulation approach for modelling and analysis of a flexible manipulator system using FE methods. In this work, a single-link flexible manipulator is considered. Using such an approach, a good approximation of the transfer function representing the actual flexible manipulator is obtained in a symbolic form. Based on these results, analyses are carried out to

investigate the relations between the physical parameters and the poles, zeros, stability, vibration frequencies and time response of the system. Experimental results using an experimental rig are presented to demonstrate the performance of the symbolic algorithm for modelling and analysis of a flexible manipulator. The rest of the paper is structured as follows: Section 2 provides a brief description of the flexible manipulator system and the FE methods considered in this study. Section 3 describes the development of the symbolic simulation algorithm. An assessment, analysis and numeric simulation of the algorithm is given in Section 4. Experimental results are presented in Section 5 and the paper is concluded in Section 6.

2. The Flexible Manipulator System And The Finite Element Method

This section describes the flexible manipulator system and the FE method used in this study. Several assumptions utilised in the process of obtaining the dynamic equations of motion of the system are briefly discussed. A description of the single-link flexible manipulator system considered in this work, is shown in Figure 1, where **XOY** and **POQ** represent the stationary and moving co-ordinates respectively, τ represents the applied torque at the hub. E, L, I, ρ, A, I_h and M_p represent the Young modulus, length, area moment of inertia, mass density per unit volume, cross sectional area, hub inertia and payload of the manipulator respectively. In this work, the motion of the manipulator is confined to the **XOY** plane. Since the manipulator is long and slender, transverse shear and rotary inertia effects are neglected. This allows the use of the Bernoulli-Euler beam theory to model the elastic behaviour of the manipulator. The manipulator is assumed to be stiff in vertical bending and torsion, allowing it to vibrate dominantly in the horizontal direction and thus, the gravity effects are neglected. Moreover, the manipulator is considered to have constant cross section and uniform material properties throughout.

The FE method has widely been used in solving material and structural problems. Since its introduction in the 1950s, the method has been continually developed and improved (Rao, 1989). The method involves decomposing a structure into several simple pieces or elements. The elements are assumed to be interconnected at certain points, known as nodes. For each element, an equation describing the behaviour of the element is obtained through an approximation technique. The elemental equations are then assembled to form the system equation. It is found that by reducing the element size of the structure, that is, increasing the number of elements, the overall solution of the system equation can be made to converge to

the exact solution. In this application, the flexible manipulator is treated as an assemblage of n elements and the development of the algorithm can be divided into four main parts: the FE analysis, state-space representation, obtaining the system transfer function and assessment of the results.

3. Development Of The Symbolic Algorithm

This section focuses on the development of the symbolic algorithm in characterising the dynamic behaviour of the flexible manipulator system. In this work, a single element of FE method is used and structural damping is ignored. Formulations to obtain the mass and stiffness matrices of the dynamic equations of motion of the system utilising the Lagrange equation are also presented. The procedure is further extended to incorporate the payload and hub inertia into the dynamic model. The equations are then expressed in a state-space form and solved to obtain the system transfer function. Two transfer functions, namely, from torque input to end-point displacement and from torque input to hub-angle of the manipulator are obtained. In this approach, all the manipulations are carried out symbolically using Macsyma, the symbolic algebraic manipulation language.

3.1 Dynamic Equations of Motion

For an angular displacement $\theta(t)$ and an elastic deflection $w(x,t)$, the total displacement $y(x,t)$ of a point along the manipulator at a distance x from the hub can be described as a function of both the rigid body motion and elastic deflection measured from the line OX as

$$y(x,t) = x\theta(t) + w(x,t) \tag{1}$$

Using the standard FE method to solve dynamic problems, leads to the well-known equation

$$w(x,t) = N_a(x)\,Q_a(t) \tag{2}$$

where $N_a(x)$ and $Q_a(t)$ represent the shape function and nodal displacement respectively. For the flexible manipulator under consideration, $w(x,t)$ in equation (2) represents the residual motion of the system. The manipulator is approximated by partitioning it into n elements. As

a consequence of using the Bernoulli-Euler beam theory, the FE method requires each node to possess two degrees of freedom, a transverse deflection and rotation. These necessitate the use of Hermite cubic basis functions as the element shape function (Ross, 1996). Hence, for the elemental length l, the shape function can be obtained as

$$N_a(x) = \left[1 - \frac{3x^2}{l^2} + \frac{2x^3}{l^3} \quad x - \frac{2x^2}{l} + \frac{x^3}{l^2} \quad \frac{3x^2}{l^2} - \frac{2x^3}{l^3} \quad -\frac{x^2}{l} + \frac{x^3}{l^2}\right]$$

For element n the nodal displacement vector is given as

$$Q_a(t) = \left[w_{n-1}(t) \quad \theta_{n-1}(t) \quad w_n(t) \quad \theta_n(t)\right]^T.$$

where $w_{n-1}(t)$ and $w_n(t)$ are the elastic deflections of the element and $\theta_{n-1}(t)$ and $\theta_n(t)$ are the corresponding angular displacement. Substituting for $w(x,t)$ from equation (2) into equation (1) and simplifying yields

$$y(x,t) = N(x)\, Q(t) \tag{3}$$

where $N(x) = \left[x \quad N_a(x)\right]$ and $Q(t) = \left[\theta(t) \quad Q_a(t)\right]^T$.

The new shape function $N(x)$ and nodal displacement vector $Q(t)$ in equation (3) incorporate local and global variables. Among these, the angle $\theta(t)$ and the distance x are global variables while $N_a(x)$ and $Q_a(t)$ are local variables. Defining $k = x - \sum_{i=1}^{n-1} l_i$ as a local variable of the nth element, where l_i is the length of the ith element, the new shape function can be expressed as

$$N(k) = \left[k + l(n-1) \quad 1 - \frac{3k^2}{l^2} + \frac{2k^3}{l^3} \quad k - \frac{2k^2}{l} + \frac{k^3}{l^2} \quad \frac{3k^2}{l^2} - \frac{2k^3}{l^3} \quad -\frac{k^2}{l} + \frac{k^3}{l^2}\right].$$

Accordingly, the kinetic energy of an element can be expressed as

$$T_n = \int_0^l \rho A \left[\frac{\partial y(k,t)}{\partial t}\right]^2 dk = \frac{1}{2}\int_0^l \rho A \dot{Y}^T \dot{Y}\, dk = \frac{1}{2}\dot{Q}^T \left[\int_0^l \rho A (N^T N)\, dk\right] \dot{Q}$$

and the potential energy of the element can be obtained as

$$P_n = \frac{1}{2}\int_0^l EI\left[\frac{\partial^2 y(k,t)}{\partial k^2}\right]^2 dk = \frac{1}{2}\int_0^l EI\,(B\,Q)^T\,(B\,Q)\,dk = \frac{1}{2}Q^T\left[\int_0^l EI\,(B^T B)\,dk\right]Q$$

where $B = \dfrac{d^2 N(k)}{dk^2} = \left[0 \quad \dfrac{12k}{l^3} - \dfrac{6}{l^2} \quad \dfrac{6k}{l^2} - \dfrac{4}{l} \quad \dfrac{6}{l^2} - \dfrac{12k}{l^3} \quad \dfrac{6k}{l^2} - \dfrac{2}{l}\right]$.

Defining M_n and K_n as

$$M_n = \int_0^l \rho A(N^T N)\ dk = \text{element mass matrix} \tag{4}$$

$$K_n = \int_0^l EI\,(B^T B)\ dk = \text{element stiffness matrix} \tag{5}$$

and solving equations (4) and (5) for the n elements, the element mass and stiffness matrices can be obtained as

$$M_n = \frac{\rho A l}{420}\begin{bmatrix} 140l(3n^2-3n+1) & 21(10n-7) & 7l(5n-3) & 21(10n-3) & -7l(5n-2) \\ 21(10n-7) & 156 & 22l & 54 & -13l \\ 7l(5n-3) & 22l & 4l^2 & 13l & -3l^2 \\ 21(10n-3) & 54 & 13l & 156 & -22l \\ -7l(5n-2) & -13l & -3l^2 & -22l & 4l^2 \end{bmatrix}$$

$$K_n = \frac{EI}{l^3}\begin{bmatrix} 0 & 0 & 0 & 0 & 0 \\ 0 & 12 & 6l & -12 & 6l \\ 0 & 6l & 4l^2 & -6l & 2l^2 \\ 0 & -12 & -6l & 12 & -6l \\ 0 & 6l & 2l^2 & -6l & 4l^2 \end{bmatrix}.$$

The matrices from above are assembled to obtain mass and stiffness matrices of the system, M and K, and used in the Lagrange equation to obtain the dynamic equation of the flexible manipulator as

$$M\ddot{Q}(t) + KQ(t) = F(t) \tag{6}$$

where $F(t)$ is the vector of applied torques and $Q(t) = [\theta \quad w_0 \quad \theta_0 \quad . \quad . \quad . \quad w_n \quad \theta_n]^T$.

Using a single element, $n = 1$, the dynamic equation of motion of the flexible manipulator can be obtained as in equation (6) where

$$M = \frac{\rho A l}{420}\begin{bmatrix} 140l^2 & 63l & 14l^2 & 147l & -21l^2 \\ 63l & 156 & 22l & 54 & -13l \\ 14l^2 & 22l & 4l^2 & 13l & -3l^2 \\ 147l & 54 & 13l & 156 & -22l \\ -21l^2 & -13l & -3l^2 & -22l & 4l^2 \end{bmatrix},$$

$$K = \frac{EI}{l^3}\begin{bmatrix} 0 & 0 & 0 & 0 & 0 \\ 0 & 12 & 6l & -12 & 6l \\ 0 & 6l & 4l^2 & -6l & 2l^2 \\ 0 & -12 & -6l & 12 & -6l \\ 0 & 6l & 2l^2 & -6l & 4l^2 \end{bmatrix},$$

$Q(t) = [\theta \quad w_0 \quad \theta_0 \quad w_1 \quad \theta_1]^T$ and $F(t) = [\tau \quad 0 \quad 0 \quad 0 \quad 0]^T$.

3.2 *Incorporation of Payload and Hub Inertia*

For the flexible manipulator under consideration, the system mass matrix can be represented as

$$M = \begin{bmatrix} M_{\theta\theta} & M_{\theta w} \\ M_{\theta w} & M_{ww} \end{bmatrix}$$

where M_{ww} is associated with the elastic degrees of freedom (residual motion), $M_{\theta w}$ represents the coupling between these elastic degrees of freedom and the hub angle θ and $M_{\theta\theta}$ is associated with the inertia of the system about the motor axis. By incorporating the payload and hub inertia of the flexible manipulator, the kinetic energy of the system can be obtained as (Azad, 1995)

$$T = \frac{1}{2}\int_0^L \rho A\left[\frac{\partial y(k,t)}{\partial t}\right]^2 dk + \frac{1}{2} I_h \dot{\theta}^2 + \frac{1}{2} M_p \left(\frac{\partial y(k,t)}{\partial t}\right)^2\Bigg|_{k=L}$$

Hence

$$T = \frac{1}{2}\int_0^L \rho A\left[\frac{\partial y(k,t)}{\partial t}\right]^2 dk + \frac{1}{2} I_h \dot{\theta}^2 + \frac{1}{2} M_p (L\dot{\theta}(t) + \dot{w}(L,t))^2$$

or

$$T = \frac{1}{2}\int_0^L \rho A\left[\frac{\partial y(k,t)}{\partial t}\right]^2 dk + \frac{1}{2}(I_h + M_p L)\dot{\theta}^2 + \frac{1}{2} M_p \dot{w}_n^2 + M_p L \dot{\theta}\dot{w}_n \qquad (7)$$

where w_n is the elastic deflection at the end-point of the manipulator.

In equation (7) the second term on the right hand side constitutes the contribution of hub inertia and payload to the rotary inertia of the system about the motor axis and contributes to the 1×1 sub-matrix $M_{\theta\theta}$. The third term demonstrates the effect of payload on the end-point residual motion of the manipulator and contributes to M_{ww} whilst the last term contributes to the coupling matrix $M_{\theta w}$. Utilising equation (7) and the FE formulation (Meirovitch, 1975), for a single element, a new system mass matrix that incorporates the hub inertia and payload can be obtained as

$$M = \frac{\rho A l}{420}\begin{bmatrix} 140l^2+m_1 & 63l & 14l^2 & 147l+m_2 & -21l^2 \\ 63l & 156 & 22l & 54 & -13l \\ 14l^2 & 22l & 4l^2 & 13l & -3l^2 \\ 147l+m_2 & 54 & 13l & 156+m_3 & -22l \\ -21l^2 & -13l & -3l^2 & -22l & 4l^2 \end{bmatrix}$$

where $m_1 = \frac{420}{\rho A l}(l^2 M_p + I_H)$, $m_2 = \frac{420}{\rho A l}(l M_p)$ and $m_3 = \frac{420}{\rho A l} M_p$.

For the manipulator considered as a pinned-free arm, with the applied torque τ at the hub, the flexural and rotational displacements, velocities and accelerations are all zero at the hub at $t = 0$. Moreover, in this work, it is assumed that $Q(0) = 0$. Incorporating the initial conditions, with flexural and rotational displacements at the hub as zero, the second and third rows and columns in M, K, Q and F are thus ignored. This yields

$$M = \frac{\rho A l}{420}\begin{bmatrix} 140l^2+m_1 & 147l+m_2 & -21l^2 \\ 147l+m_2 & 156+m_3 & -22l \\ -21l^2 & -22l & 4l^2 \end{bmatrix}, \quad K = \frac{EI}{l^3}\begin{bmatrix} 0 & 0 & 0 \\ 0 & 12 & -6l \\ 0 & -6l & 4l^2 \end{bmatrix},$$

$$Q(t) = [\theta \quad w_1 \quad \theta_1]^T \text{ and } F(t) = [\tau \quad 0 \quad 0]^T.$$

3.3 *Transfer Functions*

For control purposes, the matrix differential equation in equation (6) is represented in a state-space form as

$$\begin{aligned} \dot{v} &= \boldsymbol{A}v + \boldsymbol{B}u \\ y &= \boldsymbol{C}v + \boldsymbol{D}u \end{aligned} \tag{8}$$

where $\boldsymbol{A} = \left[\begin{array}{c|c} 0_3 & I_3 \\ \hline -M^{-1}K & 0_3 \end{array}\right]$, $\boldsymbol{B} = \left[\begin{array}{c} 0_{3\times 1} \\ \hline M_{.1}^{-1} \end{array}\right]$, $\boldsymbol{D} = [0]$.

$u = [\tau]$ and the state, $v = \left[\theta \quad w_1 \quad \theta_1 \quad \dot{\theta} \quad \dot{w}_1 \quad \dot{\theta}_1\right]^T$ that is the angular, nodal flexural and angular displacements and velocities. 0_3 is a 3×3 null matrix, $\boldsymbol{I}_3$ is a 3×3 identity matrix and $0_{3\times 1}$ is a 3×1 null vector. The output matrix $\boldsymbol{C}$ depends on desired transfer functions. For torque input to end-point displacement output, $\boldsymbol{C} = [L \quad 1 \quad 0 \quad 0 \quad 0 \quad 0]$ whilst for torque input to hub-angle output, $\boldsymbol{C} = [1 \quad 0 \quad 0 \quad 0 \quad 0 \quad 0]$.

As a result using a single element, the matrix $\boldsymbol{A}$ can be obtained as

$$\boldsymbol{A} = \begin{bmatrix} 0_3 & I_3 \\ A_{21} & 0_3 \end{bmatrix}.$$

With $\alpha = EI$ representing the flexural rigidity and $\beta = \rho A l$ representing the weight of the manipulator, the sub-matrix A_{21} can be obtained as

$$A_{21} = \frac{\beta}{\varphi}\begin{bmatrix} 0 & a_{12} & a_{13} \\ 0 & a_{22} & a_{23} \\ 0 & a_{32} & a_{33} \end{bmatrix}$$

where

$$\varphi = (15\alpha l^2 + 3600 I_H) M_P + \alpha^2 l^2 + 300\alpha I_H,$$

$$a_{12} = \frac{12(3600 l M_P + 270\alpha l)}{l^3} - \frac{6(900 M_P - 90\alpha)}{l^2},$$

$$a_{13} = \frac{4(900 M_P - 90\alpha)}{l} - \frac{6(3600 l M_P + 270\alpha l)}{l^2},$$

$$a_{22} = \frac{6(900 l^2 M_P - 15\alpha l^2 + 19800 I_H) - 12(3600 l^2 M_P + 255\alpha l^2 + 3600 I_H)}{l^3},$$

$$a_{23} = \frac{6(3600 l^2 M_P + 255\alpha l^2 + 3600 I_H) - 4(900 l^2 M_P - 15\alpha l^2 + 19800 I_H)}{l^2},$$

$$a_{32} = \frac{6(1800\alpha l^2 + 37800 I_H) M_P + 495\alpha^2 l^2 + 140400\alpha I_H}{\alpha l^4} - \frac{12(900 l^2 M_P - 15\alpha l^2 + 19800 I_H)}{l^4}$$

$$a_{33} = \frac{6(900 l^2 M_P - 15\alpha l^2 + 19800 I_H)}{l^3} - \frac{4(1800\alpha l^2 + 37800 I_H) M_P + 495\alpha^2 l^2 + 140400\alpha I_H}{\alpha l^3}.$$

Similarly, the matrix $\boldsymbol{B}$ can be obtained as

$$\boldsymbol{B} = \frac{1}{(15\alpha l^2 + 3600 I_H) M_P + \alpha^2 l^2 + 300\alpha I_H} \begin{bmatrix} 0 \\ 0 \\ 0 \\ 300\alpha + 3600 M_P \\ -270\alpha - 3600 M_P l \\ 90\alpha - 900 M_P \end{bmatrix}.$$

Using equation (8) the transfer function of the system can be expressed as

$$G(s) = \frac{Y(s)}{U(s)} = \boldsymbol{C}(s\boldsymbol{I} - \boldsymbol{A})^{-1}\boldsymbol{B} + \boldsymbol{D} \tag{9}$$

where s is the Laplace variable and $\mathbf{I}$ is the identity matrix.

For the transfer function from torque input to end-point displacement, substituting for the matrices $\mathbf{A}$, $\mathbf{B}$, $\mathbf{C}$ and $\mathbf{D}$ from equation (8) into equation (9) and simplifying yields

$$\begin{aligned} G_1(s) = {} & (30\alpha^2 l^7 s^4 - 48600\alpha\beta l^4 s^2 + 4536000\beta^2 l)/s^2[((15\alpha^2 l^8 + 3600\alpha l^6 I_H)M_P + \\ & \alpha^3 l^8 + 300\alpha^2 l^6 I_H)s^4 + ((39600\alpha\beta l^5 + 1512000\beta l^3 I_H)M_P + 5220\alpha^2\beta l^5 + \\ & 367200\alpha\beta l^3 I_H)s^2 + (4536000\beta^2 l^2 M_P + 1512000\alpha\beta^2 l^2 + 4536000\beta^2 I_H)] \end{aligned} \tag{10}$$

Similarly, the transfer function from torque input to hub-angle output of the manipulator can be obtained as

$$\begin{aligned} G_2(s) = {} & (3600\alpha l^6 M_P + 300\alpha^2 l^6)s^4 + (1512000\beta l^3 M_P + 367200\alpha\beta l^3)s^2 + 4536000\beta^2 / s^2 \\ & [((15\alpha^2 l^8 + 3600\alpha l^6 I_H)M_P + \alpha^3 l^8 + 300\alpha^2 l^6 I_H)s^4 + ((39600\alpha\beta l^5 + 1512000\beta l^3 I_H)M_P \\ & + 5220\alpha^2\beta l^5 + 367200\alpha\beta l^3 I_H)s^2 + (4536000\beta^2 l^2 M_P + 1512000\alpha\beta^2 l^2 + 4536000\beta^2 I_H)] \end{aligned} \tag{11}$$

Further, the transfer functions from torque input to end-point acceleration and hub-velocity can be obtained by differentiating $G_1(s)$ and $G_2(s)$ respectively.

4. Analysis

In this section, the transfer functions obtained in the previous section are analysed and assessed in the dynamic characterisation of the flexible manipulator system. This involves obtaining and investigating the system characteristics including poles, zeros, stability, vibration frequency and time response to an input command. Relationships between the physical parameters and the system characteristics are then investigated. Note that in this work, the

effect of damping is ignored. Therefore, the system is expected to be marginally stable, exhibiting a response of oscillatory nature.

It is noted from the transfer function $G_1(s)$ in equation (10) that the hub inertia and payload terms are not in the numerator of the transfer function. Therefore, they do not affect the system zeros. The zeros will determine whether the system exhibits minimum-phase or non-minimum phase behaviour and will determine the magnitude of response of the system. The system poles, on the other hand, are affected by the payload and the hub inertia, see equation (10). Conversely, for the transfer function $G_2(s)$ in equation (11), it is noted that the zeros are affected by the payload. Furthermore, it is noted that the flexible manipulator is a type two system, which implies that zero steady-state error can only be achieved using step and ramp command inputs to the system.

By equating the numerator of transfer function $G_1(s)$ to zero and solving yields the zeros as

$$s = \pm\frac{38.9944}{l^3}\sqrt{\frac{\beta}{\alpha}},\ s = \pm\frac{9.9718}{l^3}\sqrt{\frac{\beta}{\alpha}}$$

It is noted that, with any α, β and l values, two zeros lie on the right half of s-plane (rhp) and the others on the left half of s-plane (lhp). Thus, the system is non-minimum phase and undershoot is expected at the start in the end-point displacement response. This agrees, with the result reported earlier in respect to a system incorporating non-collocated sensors and actuators (Cannon and Schmitz, 1984; Tokhi *et al.*, 1997).

To investigate the effects of payload and hub inertia on the dynamic behaviour of the system, the transfer functions $G_1(s)$ and $G_2(s)$ were solved with a system constituting a flexible arm of dimensions $900\times3.2004\times19.008\ mm$, $E = 71\times10^9$ N/m^2, $I = 5.1924\times10^{-11}$ m^4 and ρ = 2710 kg/m^3. These parameters correspond to those of a physical flexible manipulator experimental rig, which will be introduced later in the paper. Thus, the transfer function from the torque input to end-point displacement can be obtained as

$$\begin{aligned} G_{1a}(s) = {} & (0.32s^4 - 17669.9s^2 + 5.69\times10^7)/s^2[((283.92I_H + 0.14)M_P + \\ & 3.51I_H + 0.0014)s^4 + ((4116780I_H + 12960.4)M_P + 148368.8I_H + \\ & 253.53)s^2 + (5.13\times10^7 M_P + 2535290)] \end{aligned} \qquad (12)$$

and the transfer function from torque input to hub-angle can be obtained as

$$G_{2a}(s) = ((283.86M_P + 3.51)s^4 + (4116760M_P + 148339.8)s^2 + 6.33\times10^7)/s^2$$
$$[((283.92I_H + 3.51I_H + 0.0014)s^4 + ((4116780I_H + 12960.4)M_P + \quad (13)$$
$$148368.8I_H + 253.53)s^2 + (5.13\times10^7 M_P + 2535290)]$$

By factorising the denominator of the system transfer functions $G_1(s)$ and $G_2(s)$, the system poles in terms of payload and hub inertia can be obtained as

$$s_1 = 6.09\sqrt{\frac{6.47h_1}{h_2}},\ s_2 = 6.09\sqrt{\frac{-6.47h_1}{h_2}},\ s_3 = -6.09\sqrt{\frac{6.47h_1}{h_2}},$$

$$s_4 = -6.09\sqrt{\frac{-6.47h_1}{h_2}},\ s_5 = 0,\ s_6 = 0 \quad (14)$$

where $h_1 = \sqrt{\begin{matrix}2.12\times10^8 I_H{}^2 M_P{}^2 + 605827.8 I_H M_P{}^2 + 1733.88 M_P{}^2 \\ +1.44\times10^7 I_H{}^2 M_P + 28705.3 I_H M_P + 60.47 M_P \\ +263847.6 I_H{}^2 + 490.47 I_H + 0.62)\end{matrix}} - (94119.5 I_H M_P + 296.31 M_P + 3392.06 I_H + 5.8)$

and $h_2 = 480.82 I_H M_P + 0.24 M_P + 5.95 I_H + 0.0024$.

Further, with the hub inertia $I_H = 5.8598\times10^{-4}$ kgm^2, the denominator of the system transfer functions can be obtained as

$$(0.3M_P + 0.0035)s^6 + (15370.2M_P + 340.36)s^4 + (5.13\times10^7 M_p + 2571860)s^2 \quad (15)$$

Therefore, the poles in terms of payload can be obtained as

$$s_1 = 6.09\sqrt{\frac{6.47h_3}{0.5M_P + 0.006}},\ s_2 = 6.09\sqrt{\frac{-6.47h_3}{0.5M_P + 0.006}},\ s_3 = -6.09\sqrt{\frac{6.47h_3}{0.5M_P + 0.006}}$$

$$s_4 = -6.09\sqrt{\frac{-6.47h_3}{0.5M_P + 0.006}},\ s_5 = 0,\ s_6 = 0 \quad (16)$$

where $h_3 = \sqrt{2161.6M_P{}^2 + 82.2M_P + 1.0)} - 351.5M_p - 7.8$.

Note that for a single element, the system has six poles, two of which are at the origin. Since for $M_P \geq 0$, the term in the square roots of equation (16) is negative, the remaining poles are purely imaginary and lie on the imaginary axis of the s-plane. These resulted in, as expected for a system without damping, a marginally stable system.

Thus, the system poles give the system vibration frequencies. These, in turn, determine vibration modes of the system and the effects of payload and hub inertia on the vibration

frequency can be investigated by solving equations (14) and (16). Figures 2 and 3 demonstrate the relation between payload and hub inertia with system vibration frequencies for modes 1 and 2 respectively. It is noted that with increasing payload and hub inertia, the vibration frequencies decrease significantly. These are further evidenced in Figures 4 and 5 that demonstrate the relation of payload, hub inertia and vibration frequencies for modes 1 and 2 respectively.

For the transfer function $G_2(s)$, factorising the numerator yields the zeros as

$$s_1 = \frac{3.5}{l}\sqrt{\frac{3.5\beta h_4 - 210\beta M_P - 51\alpha\beta}{12\alpha l M_P + \alpha^2 l}},\ s_2 = \frac{-3.5}{l}\sqrt{\frac{3.5\beta h_4 - 210\beta M_P - 51\alpha\beta}{12\alpha l M_P + \alpha^2 l}},$$

$$s_3 = \frac{-3.8}{l}\sqrt{\frac{12.9h_5 - 784.3M_P - 28.2672}{1.6M_P + 0.02}} \text{ and } s_4 = \frac{-3.8}{l}\sqrt{\frac{-12.9h_5 - 784.3M_P - 28.2672}{1.6M_P + 0.02}}$$

where $h_4 = \sqrt{3675M_P^2 + 1680\alpha M_P + 208\alpha^2}$ and $h_5 = \sqrt{3675M_P^2 + 249.3\alpha M_P + 4.6\alpha^2}$

Similarly, since for positive values of all parameters, the term in square roots are negative, all zeros lie on the imaginary axis. Thus, as expected of a system with collocated sensors and actuator, the transfer function from torque input to hub-angle response exhibits a minimum phase system. Figure 6 shows the relation between the system zeros and the payload. It is noted that the zeros move towards the origin of the s-plane with increasing payload.

Since control of a system with non-minimum phase characteristic is a difficult problem, this aspect is further analysed in this section. For the transfer function from the torque input to end-point displacement that shows a non-minimum phase characteristic, it is important to investigate whether the zeros can be relocated to the lhp by altering any physical parameters of the system. If so, in designing a flexible manipulator, certain parameter values can be used to make the system minimum phase. In this work, the analyses are carried out using the Routh-Hurtwiz (RH) criterion (Nise, 1995). Accordingly, if there is no sign change in the first column of RH table, then all roots of the polynomial will be on the lhp. Utilising RH criterion, the first column of RH table for numerator of $G_1(s)$ is shown in Table 1. It is noted that there are two sign changes, proving that two zeros exist on the rhp. Furthermore, the result shows that, since all terms are single, the zeros cannot be relocated by altering any parameter value.

For the transfer function $G_2(s)$, the effect of payload on the location of zeros can be investigated. Table 2 shows the first column of RH table for the numerator of $G_2(s)$. Since

the numerator is an even polynomial, a row of zeros exists at s^3. Thus, if there are no sign change, all zeros of the transfer function lie on the imaginary axis. It is noted, as all the physical parameters, including the payload are positive, no sign change occurs in the first column of RH table. This implies that all the system zeros lie on the imaginary axis and the system is minimum phase.

Similarly, the effect of payload on the system poles and stability can be studied. Furthermore, a range of payloads that ensures system stability can be determined. Table 3 shows the first column of RH table for the denominator of the transfer function, equation (15). Again, as the denominator is an even polynomial, a row of zeros exists at s^5. It is noted that, no sign change occurs. This implies that all poles of the system lie on the imaginary axis and the system is marginally stable.

The effect of payload on the dynamic behaviour of the system is further analysed by obtaining the time responses of the end-point displacement and hub-angle of the manipulator. Both transfer functions $G_1(s)$ and $G_2(s)$ are considered. In this work, a bang-bang torque is applied at the hub of the manipulator. A bang-bang torque has positive (acceleration) and negative (deceleration) period allowing the manipulator to initially accelerate and decelerate and eventually stop at a target location. The input torque can be expressed in the time-domain as

$$u(t) = ru_s(t-a) - 2ru_s(t-b) + ru_s(t-c)$$

where $u_s(t)$ is the unit step function and a, b, c and r are constants. In the frequency-domain, the input torque can be written as

$$U(s) = \frac{1}{s}(re^{-as} - 2re^{-bs} + re^{-cs}) \tag{17}$$

Multiplying the transfer functions in equations (10) and (11) with the input torque in equation (17) and utilising the inverse Laplace transform yield the time-domain expressions for the system responses. The end-point displacement, $y_1(t)$ and hub-angle, $y_2(t)$ thus obtained are given in Appendix A.

To demonstrate the performance of the developed symbolic algorithm, simulated exercises with the flexible manipulator system described in section 4 and $I_h = 5.8598 \times 10^{-4}$ kgm^2 were carried out. In these exercises, a bang-bang input torque as shown in Figure 7 with amplitude of 0.3 Nm, $a = 0.2, b = 0.5, c = 0.8$ and $r = 0.3$ was used. The system responses at the end-point and hub-angle were obtained over a period of 3 sec. Figures 8 and 9 show the

simulated responses of the end-point displacement and hub-angle respectively with a payload of 20 grams. It is noted that the responses of the system achieved steady-state values of 0.43 *m* and 28° within 0.9 *sec* with persistent oscillations. The end-point response demonstrates that the system is non-minimum phase, as the response slightly undershoots at start up. This agrees with the symbolic results that were discussed earlier.

To investigate the effect of payload on the system response, steady-state values of the system responses were monitored with various payloads. Based on the assumption, that the manipulator achieves a steady-state value after 4 sec., the relations between payload and steady-state values of end-point displacement and hub-angle are shown in Figures 10 and 11 respectively. In both cases, the output levels decrease significantly with increasing payload. The results demonstrate that controllers that are capable to adapt with changing system characteristics have to be developed.

5. Experiments

To validate the developed symbolic model of the flexible manipulator for use in simulation and control, experimental investigations using an experimental rig are carried out and the results are presented in this section. Performance of the symbolic manipulation approach is accordingly assessed by comparing the symbolic, simulation and experimental results.

5.1 The Experimental Rig

The experimental rig used in this work consists of three main parts: a flexible arm, measuring devices and a processor. A schematic diagram of the experimental rig is shown in Figure 12. The flexible arm is constructed using a piece of thin aluminium alloy with parameters as described in the earlier section. The test-rig is equipped with U9M4AT type printed circuit motor at the hub driving the flexible manipulator. The motor is chosen as the drive actuator due to its low inertia, low inductance and physical structure (PMI Motion Technologies, 1988). In this work, a linear drive amplifier LA5600 manufactured by Electro-Craft Corporation is used as a motor driver (Electrocraft Corporation, 1985). The motor drive amplifier produces a current proportional to the input voltage.

The measuring devices used in this work are the shaft encoder, tachometer and an accelerometer along the arm. The shaft encoder, with a resolution of 2048 pulses, is used for measurement of hub-angle of the manipulator. A precision interface circuit consisting of a

TCHT2000 incremental encoder interface chip and MP7636A double buffered 16 bit multiplexing digital to analogue (D/A) converter is used to convert the shaft encoder output to an analogue signal. The tachometer is used for measurement of the hub-velocity. A miniature integrated circuit piezoelectric accelerometer 303A03 is located at the end-point of the flexible arm and used for measurement of the end-point acceleration. The accelerometer has a built-in FET source follower that lowers the output impedance level. The low impedance output allows the use of long cables without an appreciable signal loss or distortion.

The processor used for this experimental rig is an IBM-PC compatible based on 486DX2 50 MHz processor. Data acquisition and control are accomplished through the utilisation of RTI - 815 I/O board. This board can provide a direct interface between the processor, actuator and sensors. The experimental set-up requires one analogue output to the motor driver amplifier and four analogue inputs from the hub- angle, hub-velocity, end-point acceleration and motor current sensor. The interface board is used with a conversion speed of 25 μ sec for A/D conversion and settling time of 20 μ sec for D/A conversion, which are adequate for the system under consideration.

5.2 *Experimental Results*

In the experiments, a bang-bang input torque as shown in Figure 7 was used. The hub-angle, hub-velocity and end-point acceleration responses were measured and the corresponding power spectral densities (SDs) were obtained. Figure 13 shows the hub-angle, hub-velocity, end-point acceleration, with the SDs, of the flexible manipulator without payload. It is noted that for the hub-angle, the steady-state level of 38° was achieved within 1.8 sec. The first three modes of vibration were obtained as 11.72 Hz, 35.15 Hz and 65.60 Hz. Furthermore, it is noted that the hub-angle response is minimum phase as proved in the analysis using symbolic manipulation. However, with a single element of FE method, the symbolic approach gave the first two modes of vibration frequencies as shown in Figure 2 as 14 Hz and 47.5 Hz. More accurate results can be obtained with increasing number of elements (Tokhi *et al.*, 1997).

To investigate the effect of payload on the performance of the manipulator, experiments were performed using various payloads ranging from 10 grams to 60 grams. Figure 14 shows the hub-angle, hub-velocity and end-point acceleration with the SDs, of the flexible manipulator with payloads of 20 grams and 60 grams. Similar to the results with symbolic manipulation, it is noted that level of hub-angle decreases with increasing payloads.

The steady-state levels of hub-angle reached 31° and 24° with a payload of 20 grams and 60 grams respectively. Moreover, a reasonably close agreement between symbolic and experimental results in the time response was achieved. Analysing the SDs, it is also noted that the resonance frequencies of the system decrease with increasing payloads. Experimental modes of vibration for the manipulator with a payload of 20 grams were obtained as 10.3 Hz, 33 Hz and 59.4 Hz. On the other hand, solving equation (16) yields the first two calculated modes of vibration as 12.6 Hz and 39.8 Hz respectively. This validates the symbolic model in characterising the dynamic behaviour of a flexible manipulator for development of suitable control strategies. However, comparing Figures 9 and 14, a difference of 3° is noted between the steady-state values of the hub-angle with payload 0f 20 grams. The difference, which is considered negligibly small, could mainly be due to the gravity effect, which was ignored in the simulation, whereas a payload that might be affected by gravity was used in the experiments. Moreover, payload rotary inertia was ignored in the simulation.

6. Conclusion

The application of a symbolic manipulation approach for modelling and analysis of a flexible manipulator system has been presented. It has been demonstrated that the approach can be utilised in characterising the dynamic behaviour of the manipulator, and to assess the stability, response and vibration frequency of the system. The system transfer functions have been obtained in a symbolic form and thus inter-relations between payload, hub inertia and system characteristics have been investigated. Simulation and experimental results have been presented demonstrating the performance of the symbolic approach in modelling and analysis of a flexible manipulator system.

7. References

AOUSTIN, Y., CHEVALLEREAU, C., GLUMINEAU, A. and MOOG, C. H. (1994). Experimental results for the end-effector control of a single flexible robotic arm, *IEEE Transactions on Control Systems Technology*, **2**(4), pp. 371-381.

AZAD, A. K. M. (1995). *Analysis and design of control mechanisms for flexible manipulator systems*, PhD. Thesis, Department of Automatic Control and Systems Engineering, The University of Sheffield, UK.

BOOK, W. J. (1984). Recursive lagrangian dynamics of flexible manipulator arms, *International Journal of Robotics Research,* **3**(3), pp. 87-101.

CANNON, R. H. and SCHMITZ, E. (1984). Initial experiment on the end-point control of a flexible one-link robot, *International Journal of Robotics Research*, **3**(3), pp. 62-75.

CETINKUNT, S. and ITTOP, B. (1992). Computer-automated symbolic modeling of dynamics of robotic manipulators with flexible links, *IEEE Transactions of Robotics and Automation*, **8**(1), pp. 94-105.

DE LUCA, A., LUCIBELLO, P. and NICOLO, F. (1988). Automatic symbolic modelling and non-linear control of robots with flexible links, *Proceedings of IEE Seminar on Robotics and Control*, Oxford, pp. 62-70.

ELECTROCRAFT CORPORATION. (1985). *DC motors speed control servo systems,* Electrocraft Corporation / Robbins & Mayers, Minnesota.

HASTING, G. G. and BOOK, W. J. (1987). A linear dynamic model for flexible robot manipulators, *IEEE Control Systems Magazine*, **7**, pp. 61-64.

LARCOMBE, P. J. and BROWN, I. C. (1997). Computer algebra: A brief overview and application to dynamic modelling, *Journal of Computing and Control Engineering*, **8**(2), pp. 53-57.

LIN, J. and LEWIS, F. L. (1994). A symbolic formulation of dynamic equations for a manipulator with rigid and flexible links, *International Journal of Robotics Research*, **13**(5), pp. 454-466.

LOW, K. H. and VIDYASAGAR, M. (1988). A Lagragian formulation of dynamic model for flexible manipulator systems, *Transactions of ASME: Journal of Dynamic Systems, Measurement and Control*, **110**, pp. 175-181.

MEIROVITCH, L. (1975). *Elements of vibration analysis*, McGraw-Hill Inc., New York.

MENQ, C. -H. and CHEN, J. -S. (1988). Dynamic modeling and payload-adaptive control of a flexible manipulator, *Proceedings of IEEE International Conference on Robotics and Automation*, Philadelphia, pp. 488-493.

NISE, N. S. (1995). *Control systems engineering*, Addison-Wesley Publishing Company, California.

PIEDBOEUF, J. -C., FAROOQ, M., BAYOUMI, M. M., LABINAZ, G. and ARGOUN, M. B. (1993). Modelling and control of flexible manipulators – Revisited, *Proceedings of 36th Midwest Symposium on Circuits and Systems*, Detroit, pp. 1480-1483.

PMI MOTION TECHNOLOGIES. (1988). *General application of printed motors,* PMI Motion Technologies, New York.

POERWANTO, H. (1998). *Dynamic simulation and control of flexible manipulator systems*, PhD. Thesis, Department of Automatic Control and Systems Engineering, The University of Sheffield, UK.

RAO, S. S. (1989). *The finite element method in engineering,* Pergamon Press, Oxford.

ROSS, C. T. F. (1996). *Finite element techniques in structural mechanics,* Albion Publishing Limited, West Sussex.

TOKHI, M. O. and AZAD, A. K. M. (1995). Real time finite difference simulation of a single-link flexible manipulator incorporating hub inertia and payload, *Proceedings of IMechE-I: Journal of Systems and Control Engineering*, **209**(I1), pp. 21-33.

TOKHI, M. O., MOHAMED, Z. and AZAD, A. K. M. (1997). Finite difference and finite element approaches to dynamic modelling of a flexible manipulator, *Proceedings of IMechE-I: Journal of Systems and Control Engineering*, **211**(I2), pp. 145-156.

TZES, A. P., YURKOVICH, S. and LANGER, F. D. (1989). A method for solution of the Euler-Bernoulli beam equation in flexible-link robotic systems, *Proceedings IEEE International Conference on Robotics and Automation*, Scottsdale, pp. 557-560.

USORO, P. B., NADIRA, R. and MAHIL, S. S. (1986). A finite element/lagrange approach to modelling lightweight flexible manipulators, *Transactions of ASME: Journal of Dynamic Systems, Measurement and Control*, **108**, pp. 198-205.

YURKOVICH, S. (1992). Flexibility effects on performance and control, *Robot Control*, IEEE Press, Part 8, pp. 321-323.

Appendix A

In this section α, β and M_P are represented as A, B and M respectively.
For *signum*, if

$$x\langle 0,\ signum(x) = -1$$

$$x = 0, signum(x) = 0$$

$$x\rangle 0,\ signum(x) = 1.$$

A1. End-point Displacement

End-point displacement, $y_1(t)$ =

```
-((sqrt(360000*M**2+84600*A*M+5889*A**2)*(31400*A*k*L**3*M**2+
12100*A**2*k*L**3*M+1106*A**3*k*L**3)*signum(t-c)+sqrt(360000*M**2+
84600*A*M+5889*A**2)*(31400*A*k*L**3*M**2+12100*A**2*k*L**3*M+1106*A**
3*k*L**3))*cos((sqrt(15*A*L*M+A**2*L)*sqrt(30*B*sqrt(360000*M**2+84600*A*M+5
889*A**2)+19800*B*M+2610*A*B)*t-c*sqrt(15*A*L*M+A**2*L)*
sqrt(30*B*sqrt(360000*M**2+84600*A*M+5889*A**2)+19800*B*M+2610*A*B))/(15*A
*L**2*M+A**2*L**2))+(sqrt(360000*M**2+84600*A*M+5889*A**2)*(-
31400*A*k*L**3*M**2-12100*A**2*k*L**3*M-1106*A**3*k*L**3)*signum(t-
c)+sqrt(360000*M**2+84600*A*M+5889*A**2)*(-31400*A*k*L**3*M**2-
12100*A**2*k*L**3*M-1106*A**3*k*L**3))*cos((sqrt(15*A*L*M+A**2*L)*sqrt(-
30*B*sqrt(360000*M**2+84600*A*M+5889*A**2)+19800*B*M+2610*A*B)*t-
c*sqrt(15*A*L*M+A**2*L)*sqrt(-30*B*sqrt(360000*M**2+84600*A*M
+5889*A**2)+19800*B*M+2610*A*B))/(15*A*L**2*M+A**2*L**2))+((-
8400000*A*k*L**3*M**3+sqrt(120000*M**2+28200*A*M+1963*A**2)*(-
15400*sqrt(3)*A*k*L**3*M**2-5770*sqrt(3)*A**2*k*L**3*M-493*sqrt(3)*A
**3*k*L**3)-4014000*A**2*k*L**3*M**2-616810*A**3*k*L**3*M-33371
*A**4*k*L**3)*signum(t-c)-8400000*A*k*L**3*M**3+sqrt(120000*M**2
+28200*A*M+1963*A**2)*(-15400*sqrt(3)*A*k*L**3*M**2-5770*sqrt(3)*A**2
*k*L**3*M-93*sqrt(3)*A**3*k*L**3)-4014000*A**2*k*L**3*M**2-616810*A
**3*k*L**3*M-33371*A**4*k*L**3)*cos((sqrt(7128000000*B*M**3+sqrt
(360000*M**2+84600*A*M+5889*A**2)*(10800000*B*M**2+2538000*A*B*M+17667
0*A**2*B)+2614680000*A*B*M**2+337408200*A**2*B*M+15370290*A**3*B)*t-
c*sqrt(7128000000*B*M**3+sqrt(360000*M**2+84600*A*M+5889*A
**2)*(10800000*B*M**2+2538000*A*B*M+176670*A**2*B)+2614680000*A*B*M**2
+337408200*A**2*B*M+15370290*A**3*B))/(L*sqrt(15*A*L*M+A**2*L)*sqrt(360000
*M**2+84600*A*M+5889*A**2)))+((-8400000*A*k*L**3*M**3+
sqrt(120000*M**2+28200*A*M+1963*A**2)*(15400*sqrt(3)*A*k*L**3*M**2+5770*sqr
t(3)*A**2*k*L**3*M+493*sqrt(3)*A**3*k*L**3)-4014000*A**2*k*L**3*M**2-
616810*A**3*k*L**3*M-33371*A**4*k*L**3)*signum(t-c)-
8400000*A*k*L**3*M**3+sqrt(120000*M**2+28200*A*M+1963*A**2)*(15400*sqrt(3)
*A*k*L**3*M**2+5770*sqrt(3)*A**2*k*L**3*M+493*sqrt(3)*A**3*k*L**3)-
4014000*A**2*k*L**3*M**2-616810*A**3*k*L**3*M-33371*A**4*k*
L**3)*cos((sqrt(7128000000*B*M**3+sqrt(360000*M**2+84600*A*M+5889*A**2)*(-
10800000*B*M**2-2538000*A*B*M-176670*A**2*B)+2614680000*A*B*M
```

2+337408200*A2*B*M+15370290*A**3*B)*t-c*sqrt(7128000000*B*M**3+
sqrt(360000*M**2+84600*A*M+5889*A**2)*(-10800000*B*M**2-2538000*Á*B *M-
176670*A**2*B)+2614680000*A*B*M**2+337408200*A**2*B*M+
15370290*A**3*B))/(L*sqrt(15*A*L*M+A**2*L)*sqrt(360000*M**2+84600*A*M+5889
*A**2)))+((-432000000*B*k*M**3-245520000*A*B*k*M**2-40906800*A**2*B*k*M-
2355600*A**3*B*k)*t**2+(864000000*B*c*k*M**3+
491040000*A*B*c*k*M**2+81813600*A**2*B*c*k*M+4711200*A**3*B*c*k)*t+(1680
0000*A*k*L**3-432000000*B*c**2*k)*M**3+(8028000*A**2*k*L**3-
245520000*A*B*c**2*k)*M**2+(1233620*A**3*k*L**3-40906800*A**2
*B*c**2*k)*M+66742*A**4*k*L**3-2355600*A**3*B*c**2*k)*signum(t-c)+(-
432000000*B*k*M**3-245520000*A*B*k*M**2-40906800*A**2*B*k*M-
2355600*A**3*B*k)*t**2+(864000000*B*c*k*M**3+491040000*A*B*c*k*M**2+8181
3600*A**2*B*c*k*M+4711200*A**3*B*c*k)*t+(16800000*A*k*L**3-
432000000*B*c**2*k)*M**3+(8028000*A**2*k*L**3-245520000*A*B*c**2*k)
*M**2+(1233620*A**3*k*L**3-40906800*A**2*B*c**2*k)*M+66742*A**4*k*L**3-
2355600*A**3*B*c**2*k)/(1728000000*B*L*M**4+1558080000*A*B*L*
M**3+490987200*A**2*B*L*M**2+63964800*A**3*B*L*M+3140800*A**4*B*L)+2*(
(sqrt(360000*M**2+84600*A*M+5889*A**2)*(31400*A*k*L**3*M**2+12100*A**2*k*
L**3*M+1106*A**3*k*L**3)*signum(t-b)+sqrt(360000*M**2+
84600*A*M+5889*A**2)*(31400*A*k*L**3*M**2+12100*A**2*k*L**3*M+1106*A**
3*k*L**3))*cos((sqrt(15*A*L*M+A**2*L)*sqrt(30*B*sqrt(360000*M**2+84600*A*M+5
889*A**2)+19800*B*M+2610*A*B)*t-b*sqrt(15*A*L*M+A**2*
L)*sqrt(30*B*sqrt(360000*M**2+84600*A*M+5889*A**2)+19800*B*M+2610*A*B))/(1
5*A*L**2*M+A**2*L**2))+(sqrt(360000*M**2+84600*A*M+5889*A**2)*(-
31400*A*k*L**3*M**2-12100*A**2*k*L**3*M-1106*A**3*k*L**3)*signum(t-
b)+sqrt(360000*M**2+84600*A*M+5889*A**2)*(-31400*A*k*L**3*M**2-
12100*A**2*k*L**3*M-1106*A**3*k*L**3))*cos((sqrt(15*A*L*M+A**2*L)*sqrt(-
30*B*sqrt(360000*M**2+84600*A*M+5889*A**2)+19800*B*M+2610*A*B)*t-
b*sqrt(15*A*L*M+A**2*L)*sqrt(-30*B*sqrt(360000*M**2+
84600*A*M+5889*A**2)+19800*B*M+2610*A*B))/(15*A*L**2*M+A**2*L**2))+((-
8400000*A*k*L**3*M**3+sqrt(120000*M**2+28200*A*M+1963*A**2)*(-
15400*sqrt(3)*A*k*L**3*M**2-5770*sqrt(3)*A**2*k*L**3*M-493*sqrt(3)*A**
3*k*L**3)-4014000*A**2*k*L**3*M**2-616810*A**3*k*L**3*M-33371*A**4
*k*L**3)*signum(t-b)-8400000*A*k*L**3*M**3+sqrt(120000*M**2+28200*A*
M+1963*A**2)*(-15400*sqrt(3)*A*k*L**3*M**2-5770*sqrt(3)*A**2*k*L**3*M-
493*sqrt(3)*A**3*k*L**3)-4014000*A**2*k*L**3*M**2-616810*A**3*k*L**3*M-
33371*A**4*k*L**3)*cos((sqrt(7128000000*B*M**3+sqrt(360000*M**2
+84600*A*M+5889*A**2)*(10800000*B*M**2+2538000*A*B*M+176670*A**2*B)+26
14680000*A*B*M**2+337408200*A**2*B*M+15370290*A**3*B)*t-b*
sqrt(7128000000*B*M**3+sqrt(360000*M**2+84600*A*M+5889*A**2)*(10800000*B*
M**2+2538000*A*B*M+176670*A**2*B)+2614680000*A*B*M**2+337408200*A**2*
B*M+15370290*A**3*B))/(L*sqrt(15*A*L*M+A**2*L)*sqrt(360000*M**2+84600*A*M
+5889*A**2)))+((-8400000*A*k*L**3*M**3+sqrt(120000*
M**2+28200*A*M+1963*A**2)*(15400*sqrt(3)*A*k*L**3*M**2+5770*sqrt(3)*A**2*k
*L**3*M+493*sqrt(3)*A**3*k*L**3)-4014000*A**2*k*L**3*M**2-
616810*A**3*k*L**3*M-33371*A**4*k*L**3)*signum(t-b)-8400000*A*k*L
3*M3+sqrt(120000*M**2+28200*A*M+1963*A**2)*(15400*sqrt(3)*A*k*L**3*M*
*2+5770*sqrt(3)*A**2*k*L**3*M+493*sqrt(3)*A**3*k*L**3)-4014000*
A**2*k*L**3*M**2-616810*A**3*k*L**3*M-33371*A**4*k*L**3)*cos((sqrt

```
(7128000000*B*M**3+sqrt(360000*M**2+84600*A*M+5889*A**2)*(-
10800000*B*M**2-2538000*A*B*M-176670*A**2*B)+2614680000*A*B*M**2
+337408200*A**2*B*M+15370290*A**3*B)*t-b*sqrt(7128000000*B*M**3+sqrt
(360000*M**2+84600*A*M+5889*A**2)*(-10800000*B*M**2-2538000*A*B*M-
176670*A**2*B)+2614680000*A*B*M**2+337408200*A**2*B*M+15370290*
A**3*B))/(L*sqrt(15*A*L*M+A**2*L)*sqrt(360000*M**2+84600*A*M+5889*A**2)))+(
(-432000000*B*k*M**3-245520000*A*B*k*M**2-40906800*A**2*B*k*M-
2355600*A**3*B*k)*t**2+(864000000*b*B*k*M**3+491040000*A*b*B*k
*M**2+81813600*ALPHA**2*b*B*k*M+4711200*A**3*b*B*k)*t+(16800000*A*k*L**
3-432000000*b**2*B*k)*M**3+(8028000*A**2*k*L**3-245520000*A
*b**2*B*k)*M**2+(1233620*A**3*k*L**3-40906800*A**2*b**2*B*k)*M+
66742*A**4*k*L**3-2355600*A**3*b**2*B*k)*signum(t-b)+(-432000000*B*k*M**3-
245520000*A*B*k*M**2-40906800*A**2*B*k*M-2355600*A**3*B*k)
*t**2+(864000000*b*B*k*M**3+491040000*A*b*B*k*M**2+81813600*A**2*b*B*k*
M+4711200*A**3*b*B*k)*t+(16800000*A*k*L**3-432000000*b**2*B
*k)*M**3+(8028000*A**2*k*L**3-245520000*A*b**2*B*k)*M**2+(1233620*
A**3*k*L**3-40906800*A**2*b**2*B*k)*M+66742*A**4*k*L**3-2355600*A
**3*b**2*B*k)/(1728000000*B*L*M**4+1558080000*A*B*L*M**3+490987200*A**2*
B*L*M**2+63964800*A**3*B*L*M+3140800*A**4*B*L)-(sqrt(360000*
M**2+84600*A*M+5889*A**2)*(((31400*A*k*L**3*M**2+12100*A**2*k*L**3*M+11
06*A**3*k*L**3)*signum(t-a)+31400*A*k*L**3*M**2+12100*A**2*k
*L**3*M+1106*A**3*k*L**3)*cos(sqrt(15*A*L*M+A**2*L)*sqrt(30*B*sqrt(360000*M
**2+84600*A*M+5889*A**2)+19800*B*M+2610*A*B)*(t-a)/(15*A*L**
2*M+A**2*L**2))+((-31400*A*k*L**3*M**2-12100*A**2*k*L**3*M-1106*A
**3*k*L**3)*signum(t-a)-31400*A*k*L**3*M**2-12100*A**2*k*L**3*M-1106
*A**3*k*L**3)*cos(sqrt(15*A*L*M+A**2*L)*sqrt(-30*B*sqrt(360000*M**2+
84600*A*M+5889*A**2)+19800*B*M+2610*A*B)*(t-a)/(15*A*L**2*M+A**2*L
**2)))+sqrt(120000*M**2+28200*A*M+1963*A**2)*(((-15400*sqrt(3)*A*k*L**3
*M**2-5770*sqrt(3)*A**2*k*L**3*M-493*sqrt(3)*A**3*k*L**3)*signum(t-a)-
15400*sqrt(3)*A*k*L**3*M**2-5770*sqrt(3)*A**2*k*L**3*M-493*sqrt(3)*A**
3*k*L**3)*cos(sqrt(7128000000*B*M**3+sqrt(360000*M**2+84600*A*M+5889*A**2)*
(10800000*B*M**2+2538000*A*B*M+176670*A**2*B)+2614680000*A*B*M**2+3374
08200*A**2*B*M+15370290*A**3*B)*(t-a)/(L*sqrt(15*A*L*M+
A**2*L)*sqrt(360000*M**2+84600*A*M+5889*A**2)))+((15400*sqrt(3)*A*k*L**3*M*
*2+5770*sqrt(3)*A**2*k*L**3*M+493*sqrt(3)*A**3*k*L**3)*signum(t-
a)+15400*sqrt(3)*A*k*L**3*M**2+5770*sqrt(3)*A**2*k*L**3*M+493*sqrt(3)*A**3*k*
L**3)*cos(sqrt(7128000000*B*M**3+sqrt(360000*M**2+84600*A*M+5889*A**2)*(-
10800000*B*M**2-2538000*A*B*M-176670*A**2*B)+2614680000
*A*B*M**2+337408200*A**2*B*M+15370290*A**3*B)*(t-a)/(L*sqrt(15*A*L*
M+A**2*L)*sqrt(360000*M**2+84600*A*M+5889*A**2))))+((-8400000*A*k*L
**3*M**3-4014000*A**2*k*L**3*M**2-616810*A**3*k*L**3*M-33371*A**4
*k*L**3)*signum(t-a)-8400000*A*k*L**3*M**3-4014000*A**2*k*L**3*M**2-
616810*A**3*k*L**3*M-33371*A**4*k*L**3)*cos(sqrt(7128000000*B*M**3+
sqrt(360000*M**2+84600*A*M+5889*A**2)*(10800000*B*M**2+2538000*A*B*M+17
6670*A**2*B)+2614680000*A*B*M**2+337408200*A**2*B*M+15370290*A**3*B)*(t-
a)/(L*sqrt(15*A*L*M+A**2*L)*sqrt(360000*M**2+84600*A*M+ 5889*A**2)))+((-
8400000*A*k*L**3*M**3-4014000*A**2*k*L**3*M**2-616810*A**3*k*L**3*M-
33371*A**4*k*L**3)*signum(t-a)-8400000*A*k*L**3 *M**3-
4014000*A**2*k*L**3*M**2-616810*A**3*k*L**3*M-33371*A**4*k*
```

L**3)*cos(sqrt(7128000000*B*M**3+sqrt(360000*M**2+84600*A*M+5889*A**2)*(-
10800000*B*M**2-2538000*A*B*M-176670*A**2*B)+2614680000*A*B*M
2+337408200*A2*B*M+15370290*A**3*B)*(t-a)/(L*sqrt(15*A*L*M+A**2*
L)*sqrt(360000*M**2+84600*A*M+5889*A**2)))+((-432000000*B*k*M**3-
245520000*A*B*k*M**2-40906800*A**2*B*k*M-2355600*A**3*B*k)*t**2+
(864000000*a*B*k*M**3+491040000*a*A*B*k*M**2+81813600*a*A**2*B*k*M+4711
200*a*A**3*B*k)*t+(16800000*A*k*L**3-432000000*a**2*B*k)*M
3+(8028000*A2*k*L**3-245520000*a**2*A*B*k)*M**2+(1233620*A**3* k*L**3-
40906800*a**2*A**2*B*k)*M+66742*A**4*k*L**3-2355600*a**2*A
3*B*k)*signum(t-a)+(-432000000*B*k*M3-245520000*A*B*k*M**2-
40906800*A**2*B*k*M-2355600*A**3*B*k)*t**2+(864000000*a*BA*k*M**3+
491040000*a*A*B*k*M**2+81813600*a*A**2*B*k*M+4711200*a*A**3*B*k)*t+(1680
0000*A*k*L**3-432000000*a**2*B*k)*M**3+(8028000*A**2*k*L **3-
245520000*a**2*A*B*k)*M**2+(1233620*A**3*k*L**3-40906800*a**2*A**2*
B*k)*M+66742*A**4*k*L**3-2355600*a**2*A**3*B*k)/(1728000000*B*L*M**
4+1558080000*A*B*L*M**3+490987200*A**2*B*L*M**2+63964800*A**3*B*L*M+3
140800*A**4*B*L)

A2. The hub-angle

The hub-angle output in the time-domain, $y_2(t)$ can be obtained as

$$y_2(t) = y_2(t,a) - 2y_2(t,b) + y_2(t,c)$$

where

$y_2(t,a) =$
(sqrt(360000*M**2+84600*A*M+5889*A**2)*(((384000*k*L**3*M**3+252600*A*k*L
3*M2+55440*A**2*k*L**3*M+4074*A**3*k*L**3)*signum(t-a)+
384000*k*L**3*M**3+252600*A*k*L**3*M**2+55440*A**2*k*L**3*M+
4074*A**3*k*L**3)*cos(sqrt(15*A*L*M+A**2*L)*sqrt(30*B*sqrt(360000*M**2+84600
*A*M+5889*A**2)+19800*B*M+2610*A*BETA)*(t-a)/(15*A*L**2*M+
A**2*L**2))+((-384000*k*L**3*M**3-252600*A*k*L**3*M**2-55440*A**2*k *L**3*
M-4074*ALPHA**3*k*L**3)*signum(t-a)-384000*k*L**3*M**3-252600
*A*k*L**3*M**2-55440*A**2*k*L**3*M-4074*A**3*k*L**3)*cos(sqrt(15*A*
L*M+A**2*L)*sqrt(-30*B*sqrt(360000*M**2+84600*A*M+5889*A**2)+19800*
B*M+2610*A*B)*(t-a)/(15*A*L**2*M+A**2*L**2)))+sqrt(120000*M**2+28200
*ALPHA*M+1963*A**2)*(((-264000*sqrt(3.0)*k*L**3*M**3-180000*sqrt(3.0)*A
*k*L**3*M**2-39600*sqrt(3.0)*A**2*k*L**3*M-2697*sqrt(3.0)*A**3*k*L**3)*
signum(t-a)-264000*sqrt(3.0)*k*L**3*M**3-180000*sqrt(3.0)*A*k*L**3*M**2-
39600*sqrt(3.0)*A**2*k*L**3*M-2697*sqrt(3.0)*A**3*k*L**3)*cos(sqrt
(7128000000*B*M**3+sqrt(360000*M**2+84600*A*M+5889*A**2)*(10800000*B*M**
2+2538000*A*BETA*M+176670*A**2*B)+2614680000*A*B*M**2+337408200*A**2*
B*M+15370290*A**3*B)*(t-a)/(L*sqrt(15*A*L*M+A**2*L)*sqrt
(360000*M**2+84600*A*M+5889*A**2)))+((264000*sqrt(3.0)*k*L**3*M**3+180000*s
qrt(3.0)*A*k*L**3*M**2+39600*sqrt(3.0)*A**2*k*L**3*M+2697*sqrt(3.0)*A**3*k*L*
*3)*signum(t-a)+264000*sqrt(3.0)*k*L**3*M**3+180000*sqrt(3.0)*

A*k*L**3*M**2+39600*sqrt(3.0)*A**2*k*L**3*M+2697*sqrt(3.0)*A**3*k*L**3)*cos(s
qrt(7128000000*B*M**3+sqrt(360000*M**2+84600*A*M+5889*A**2)*(-
10800000*B*M**2-2538000*A*B*M-176670*A**2*B)+2614680000*A*B*M**
2+337408200*A**2*B*M+15370290*A**3*B)*(t-a)/(L*sqrt(15*A*L*M+A**2*L)
*sqrt(360000*M**2+84600*A*M+5889*A**2))))+((-144000000*k*L**3*M**4-
113040000*A*k*L**3*M**3-32127600*A**2*k*L**3*M**2-3918180*A**3*k*L
3*M-182559*A4*k*L**3)*signum(t-a)-144000000*k*L**3*M**4-113040000
*A*k*L**3*M**3-32127600*A**2*k*L**3*M**2-3918180*A**3*k*L**3*M-
182559*A**4*k*L**3)*cos(sqrt(7128000000*B*M**3+sqrt(360000*M**2+84600*A*M+
5889*A**2)*(10800000*B*M**2+2538000*A*B*M+176670*A**2*B)+2614680000*A*B
*M**2+337408200*A**2*B*M+15370290*A**3*B)*(t-a)/(L*sqrt
(15*A*L*M+A**2*L)*sqrt(360000*M**2+84600*A*M+5889*A**2)))+((-
144000000*k*L**3*M**4-113040000*A*k*L**3*M**3-32127600*A**2*k*L**3 *M**2-
3918180*A**3*k*L**3*M-182559*A**4*k*L**3)*signum(t-a)-144000000
*k*L**3*M**4-113040000*A*k*L**3*M**3-32127600*A**2*k*L**3*M**2-
3918180*A**3*k*L**3*M-182559*A**4*k*L**3)*cos(sqrt(7128000000*B*M**3
+sqrt(360000*M**2+84600*A*M+5889*ALPHA**2)*(-10800000*B*M**2-
2538000*A*B*M-176670*A**2*B)+2614680000*A*B*M**2+337408200*A**2*
B*M+15370290*A**3*B)*(t-a)/(L*sqrt(15*A*L*M+A**2*L)*sqrt(360000*M**2+
84600*A*M+5889*A**2)))+((432000000*B*k*M**3+245520000*A*B*k*M**2+4090680
0*A**2*BETA*k*M+2355600*A**3*B*k)*t**2+(-864000000*a*B*k*M**3-
491040000*A*A*B*k*M**2-81813600*A*A**2*B*k*M-4711200*A*A**3*B
*k)*t+288000000*k*L**3*M**4+(226080000*A*k*L**3+432000000*A**2*B*k)*M**3+
(64255200*A**2*k*L**3+245520000*A**2*A*B*k)*M**2+(7836360*A**3*k*L**3+40
906800*A**2*A**2*B*k)*M+365118*A**4*k*L**3+2355600*A**2*A**3*B*k)*signum
(t-a)+(432000000*B*k*M**3+245520000*A*B*k*M**2+
40906800*A**2*B*k*M+2355600*A**3*B*k)*t**2+(-864000000*A*B*k*M**3-
491040000*A*A*B*k*M**2-81813600*A*A**2*B*k*M-4711200*A*A**3*B*k)
*t+288000000*k*L**3*M**4+(226080000*A*k*L**3+432000000*A**2*B*k)*M**3+(64
255200*A**2*k*L**3+245520000*A**2*A*B*k)*M**2+(7836360*A**3*k*L**3+40906
800*A**2*A**2*B*k)*M+365118*A**4*k*L**3+2355600*A**2*A**3*B*k)/(17280000
00*B*L**2*M**4+1558080000*A*B*L**2*M**3+490987200*A**2*B*L**2*M**2+639
64800*A**3*B*L**2*M+3140800*A**4*B*L**2)

Similarly, $y_2(t,b)$ and $y_2(t,c)$ can be obtained by replaciing a with b and c respectively in the above expression.

TABLES

Table 1: The first column of RH table for the numerator of $G_1(s)$.	
s^4	$30\alpha^2 l^7$
s^3	$120\alpha^2 l^7$
s^2	$-24300\alpha\beta l^4$
s^1	$-74800\alpha\beta l^4$
s^0	$4536000\beta^2 l$

Table 2: The first column of RH table for the numerator of $G_2(s)$.	
s^4	$30\alpha l^6(12M_P+\alpha)$
s^3	$120\alpha l^6(12M_P+\alpha)$
s^2	$10800\beta l^3(17\alpha+70M_P)$
s^1	$\dfrac{57600(\beta l^3(17\alpha+70M_P)}{17\alpha+70M_P}$
s^0	$4536000\beta^2$

Table 3: The first column of RH table for denominator of the system.	
s^6	$0.3M_P+0.0035$
s^5	$1.9M_P+0.0208$
s^4	$5123.4M_P+113.5$
s^3	$\dfrac{7.6\times10^8 M_P{}^2+3.0\times10^7 M_P+356584.8}{15370.2M_P+340.4}$
s^2	$\dfrac{1.4\times10^{27}M_P{}^3+1.3\times10^{26}M_P{}^2+3.4\times10^{24}M_P+3.3\times10^{22}}{6.1\times10^{19}M_P{}^2+2.4\times10^{18}M_P+2.8\times10^{16}}$
s^1	$1.0\times10^8 M_P+5143720$
s^0	0

FIGURES

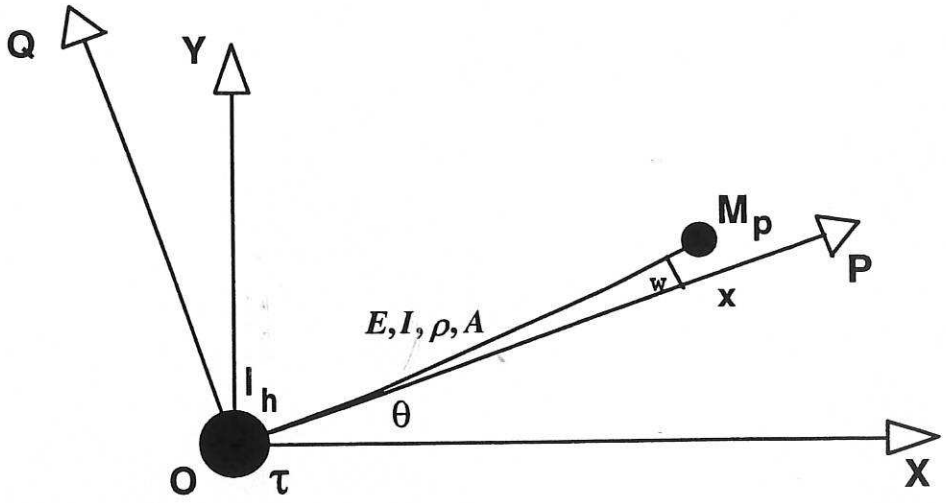

Figure 1. Description of the flexible manipulator system.

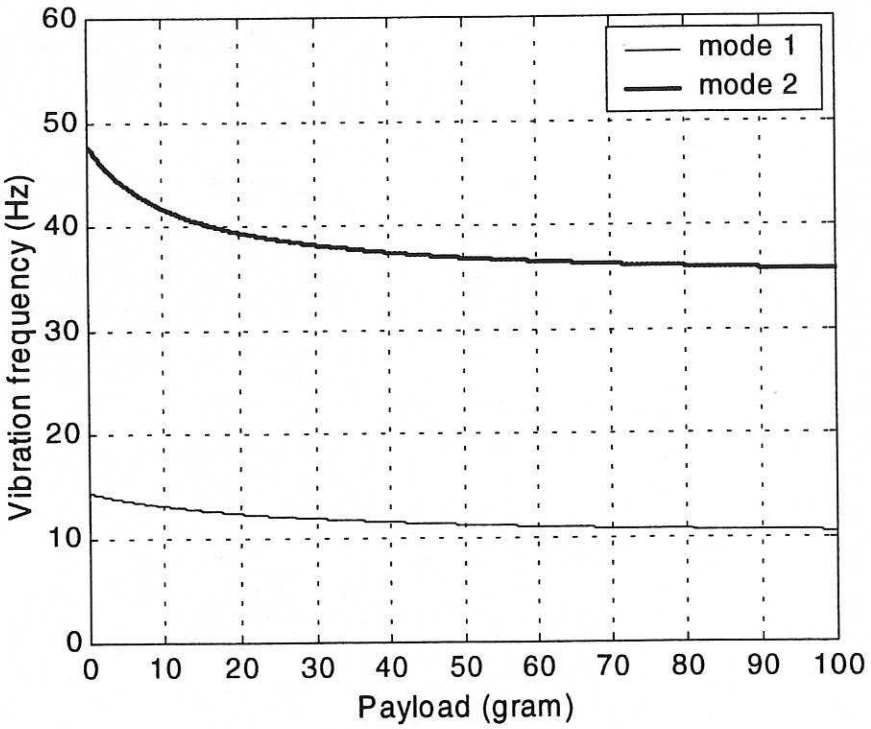

Figure 2. Effect of payload on the vibration frequency of the end-point response using $I_H = 5.8598 \times 10^{-4}\ kgm^2$.

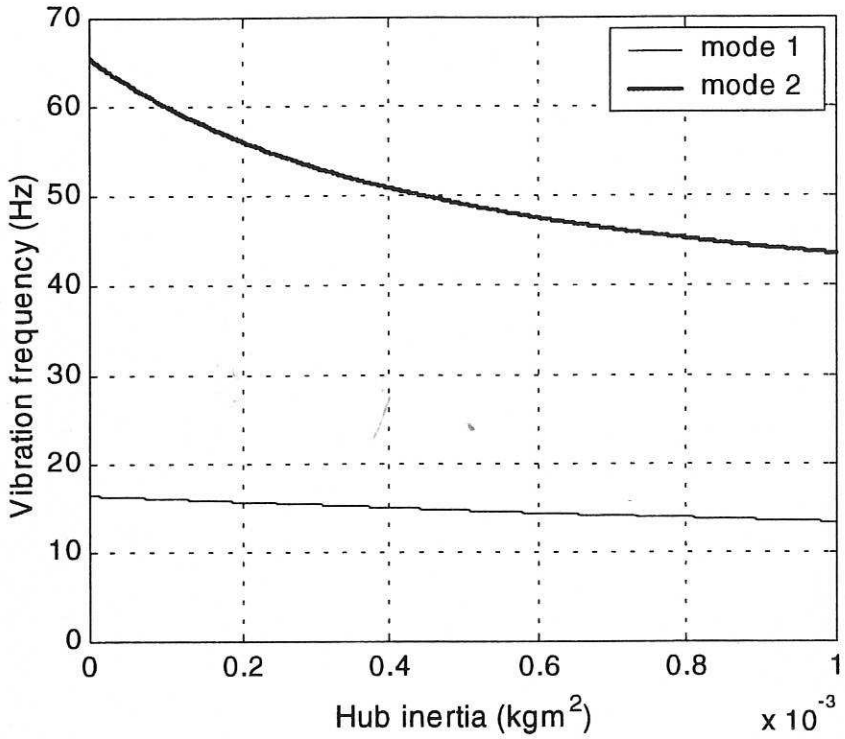

Figure 3. Effect of hub inertia on the vibration frequency of the end-point response using $M_p = 30$ grams.

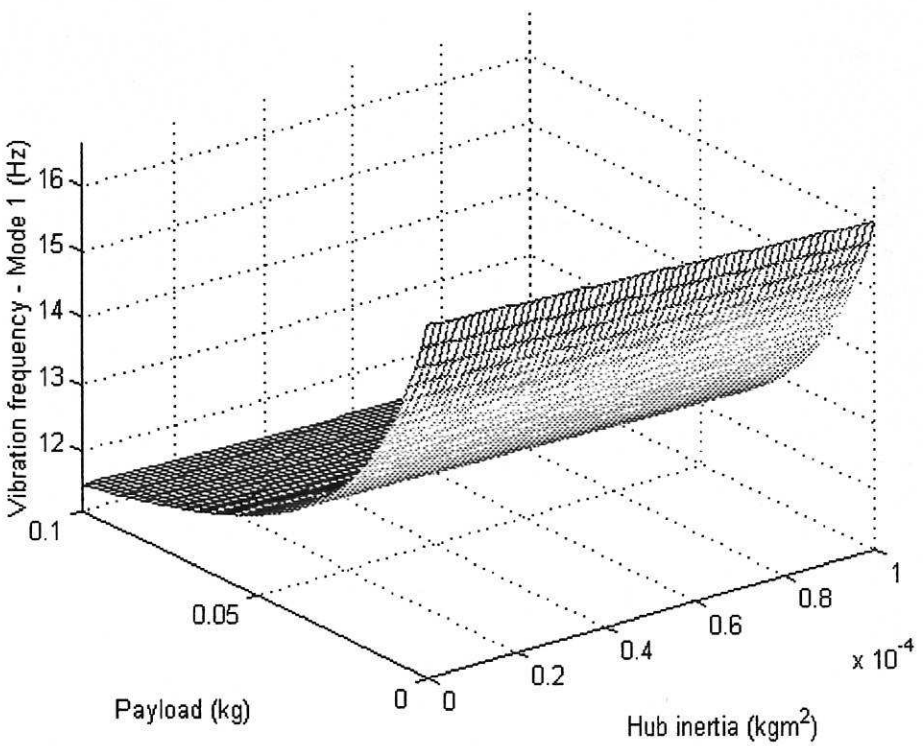

Figure 4. Relationship between hub inertia, payload and vibration frequency of mode 1.

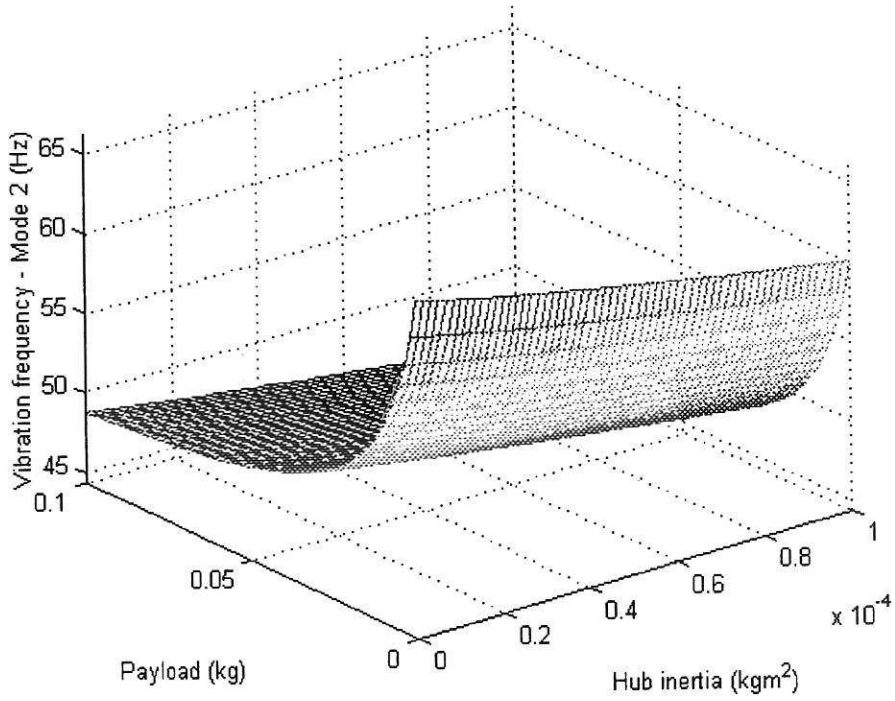

Figure 5. Relationship between hub inertia, payload and vibration frequency of mode 2.

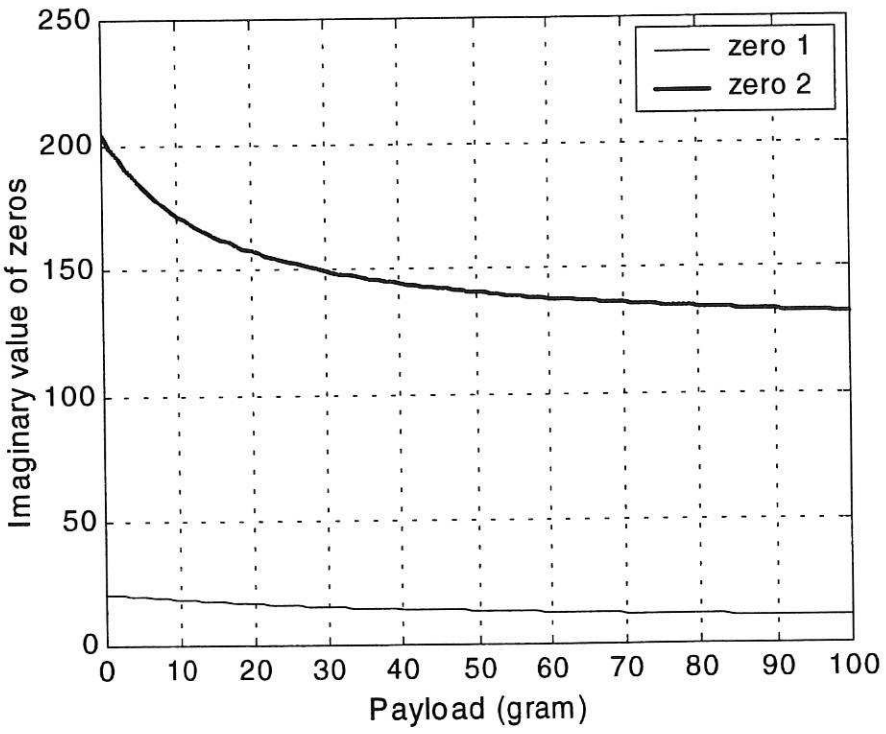

Figure 6. Effect of payload on the zeros of hub-angle response.

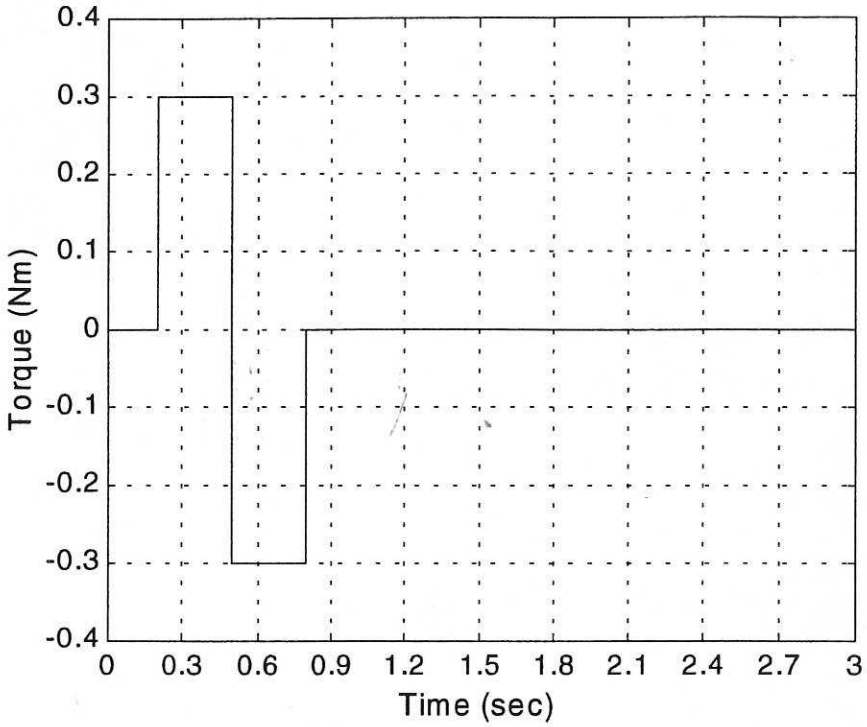

Figure 7. The bang-bang input torque.

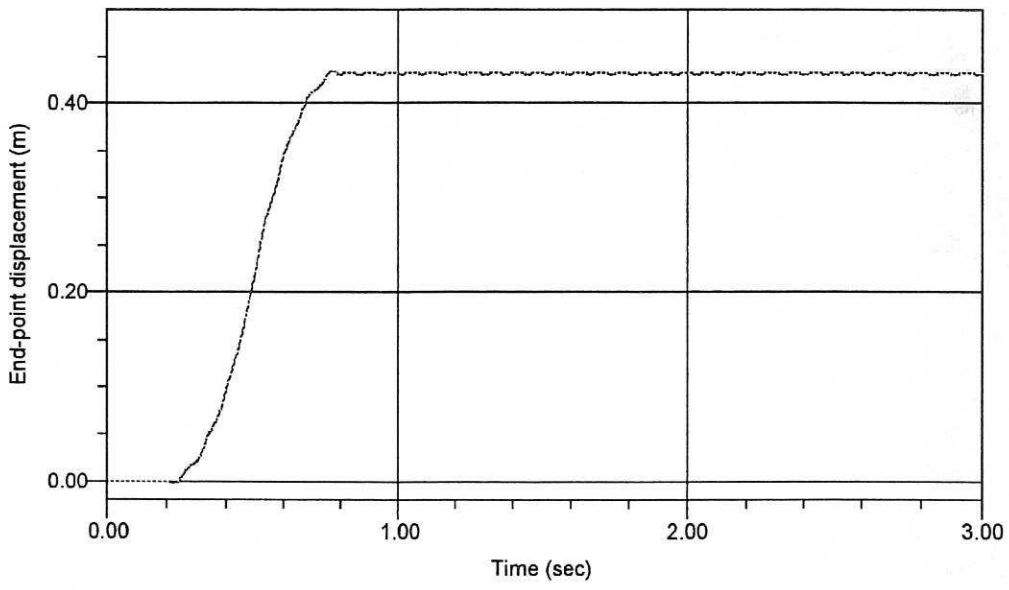

Figure 8. Simulated end-point displacement response of the flexible manipulator ($M_p = 20$ grams).

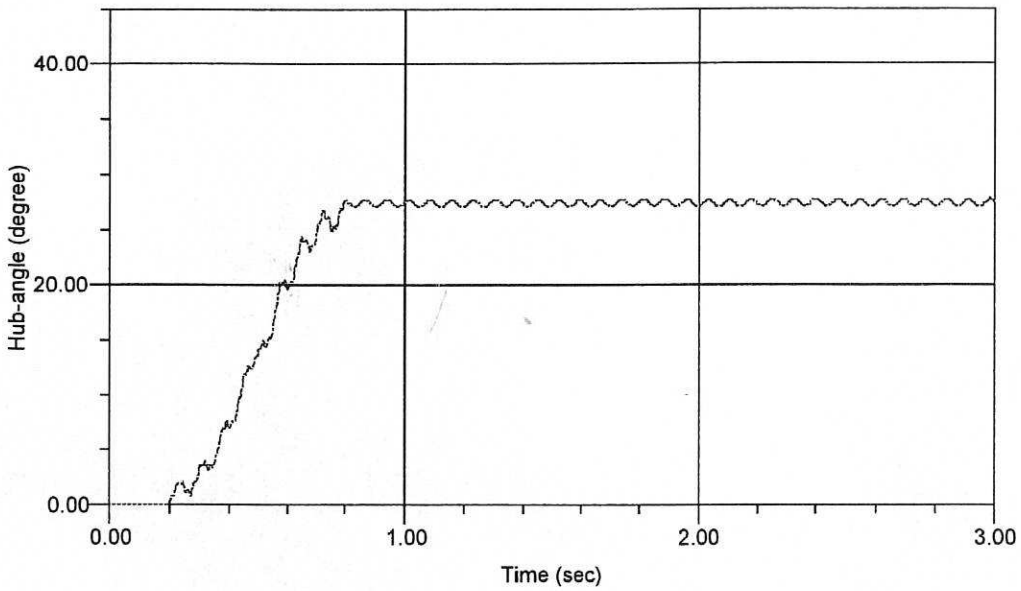

Figure 9. Simulated hub-angle response of the flexible manipulator ($M_p = 20$ grams).

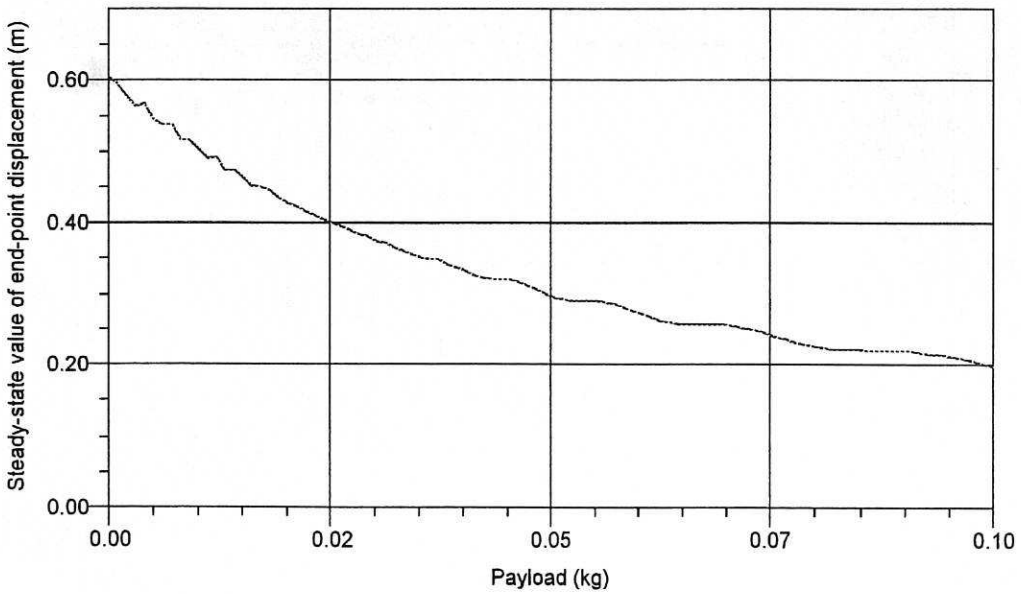

Figure 10. Effect of payload on the steady-state value of end-point displacement response ($t = 4$ sec).

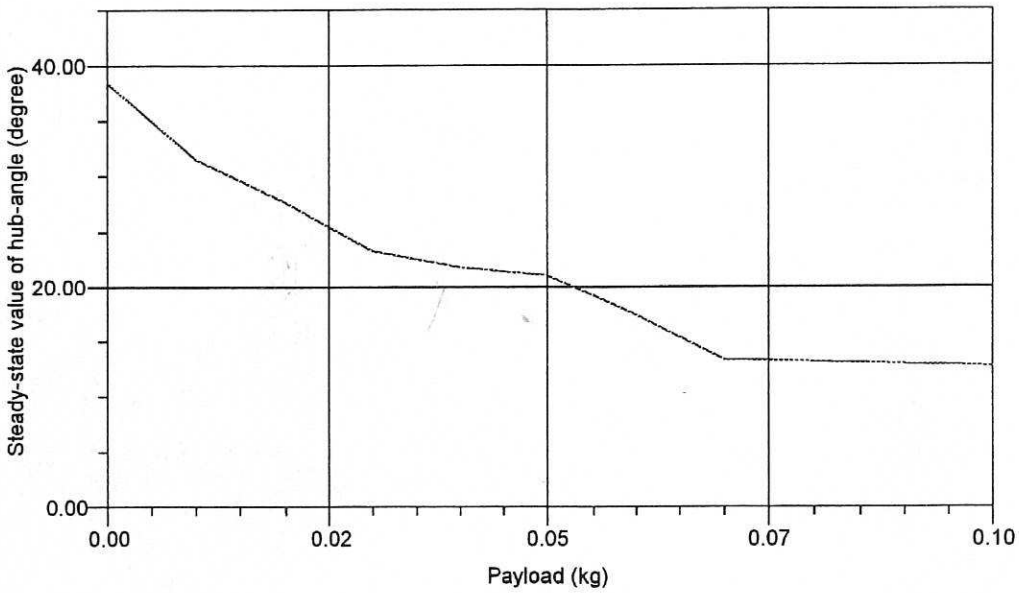

Figure 11. Effect of payload on the steady-state value of hub-angle response ($t = 4$ sec).

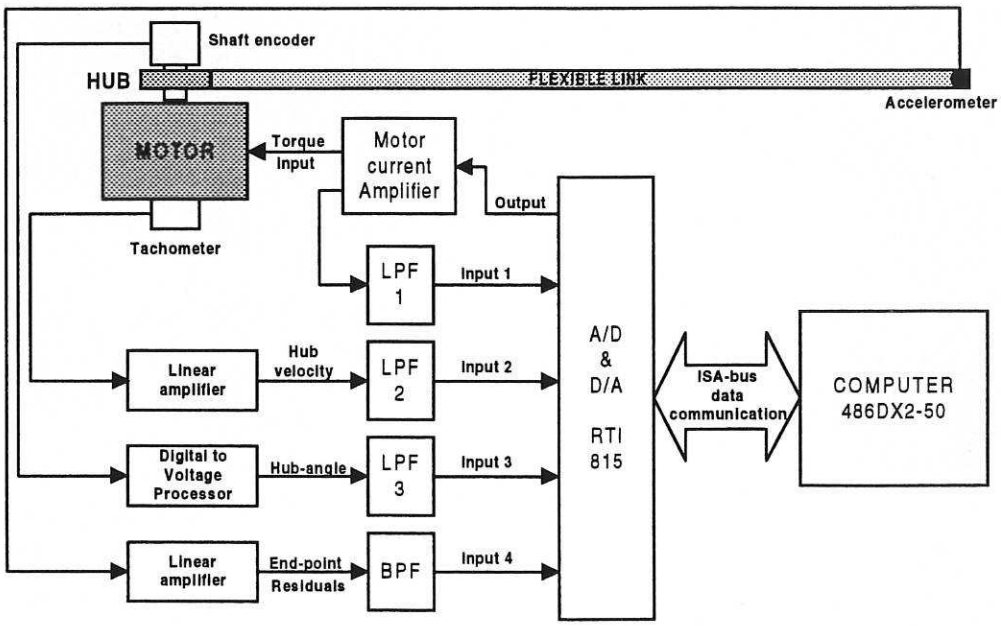

Figure 12. Schematic diagram of the experimental rig.

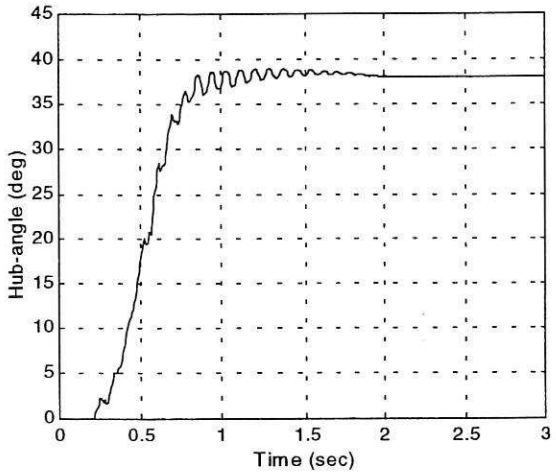

(a) Hub-angle.

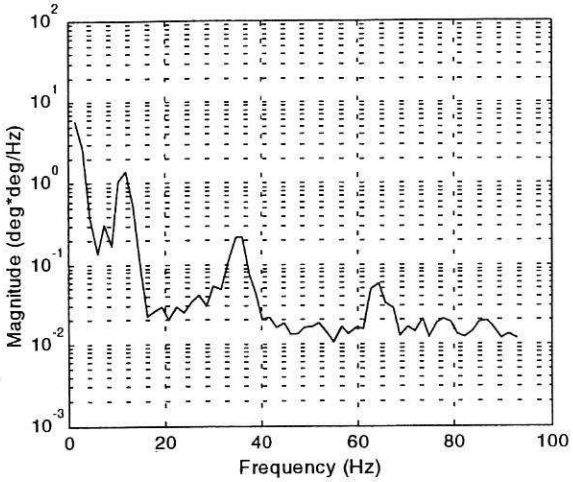

(b) SD of hub-angle.

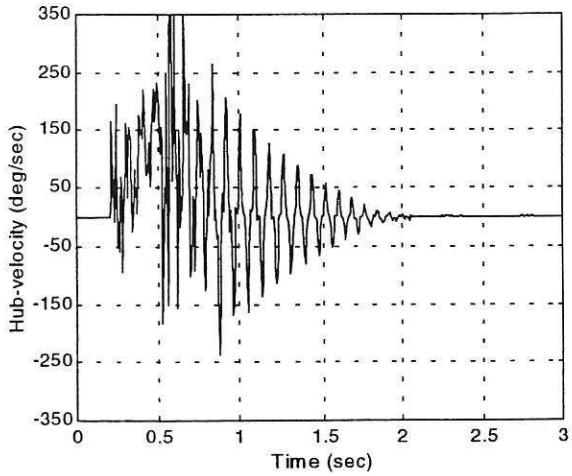

(c) Hub-velocity.

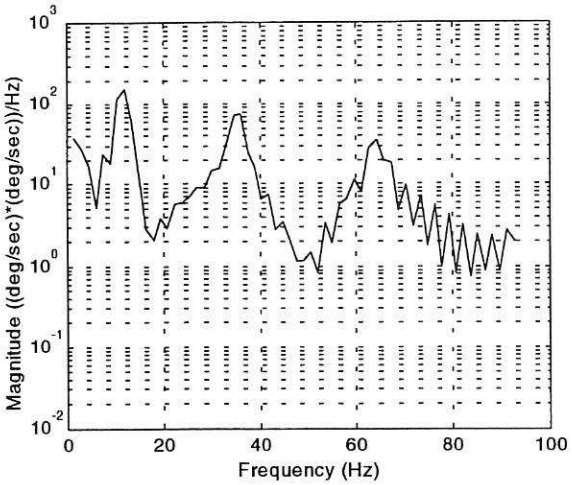

(d) SD of hub-velocity.

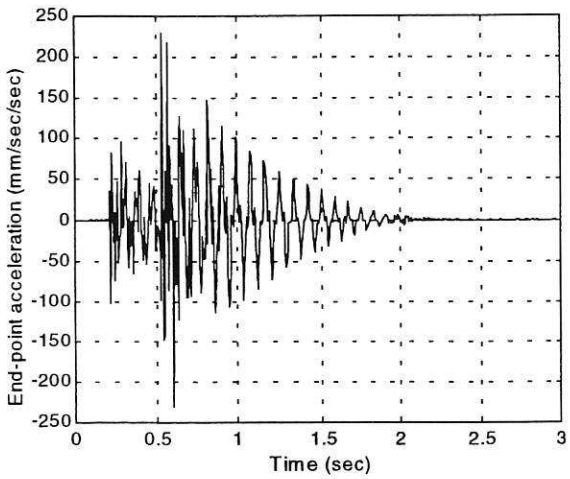

(e) End-point acceleration.

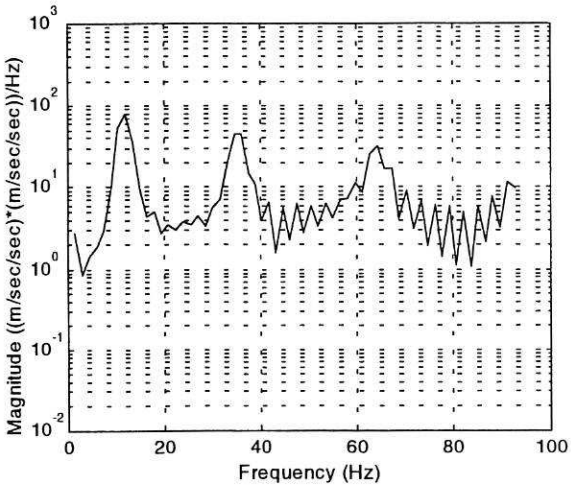

(f) SD of end-point acceleration.

Figure 13. Response of the flexible manipulator experimental rig without payload.

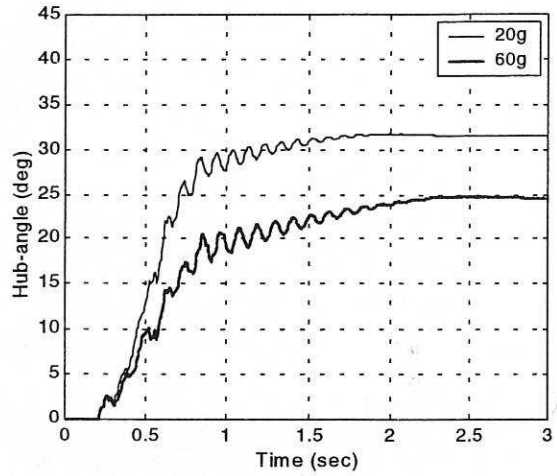

(a) Hub-angle.

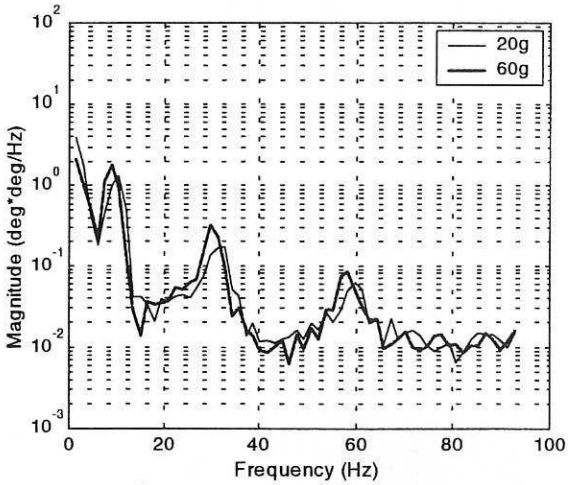

(b) SD of hub-angle.

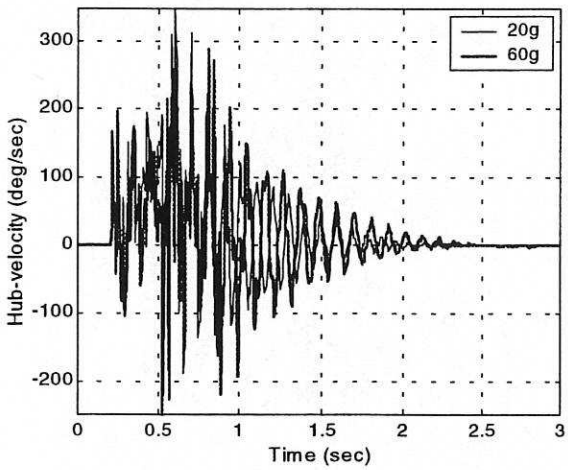

(c) Hub-velocity.

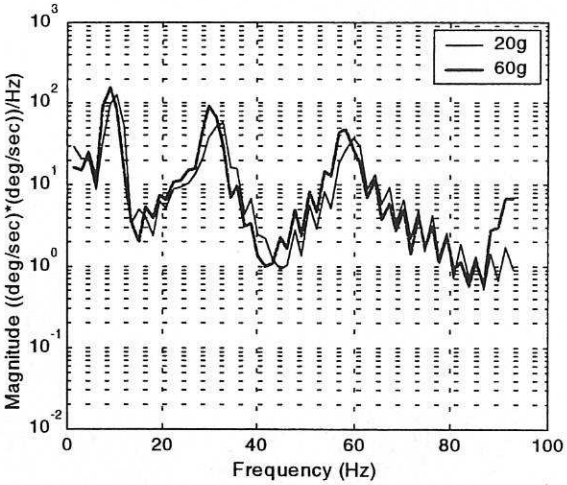

(d) SD of hub-velocity.

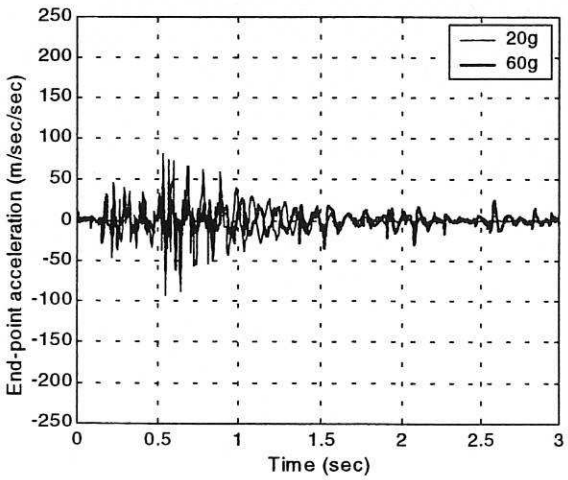

(e) End-point acceleration.

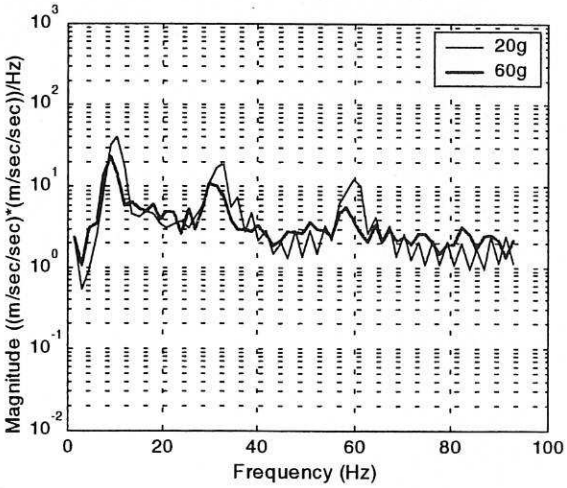

(f) SD of end-point acceleration.

Figure 14. Response of the flexible manipulator experimental rig with payloads of 20 grams and 60 grams.